1

2

3 **Stem cell niche signals Wnt, Hedgehog, and Notch distinctively regulate Drosophila follicle**

4 **precursor cell differentiation**

5

6 Wei Dai, Amy Peterson, Thomas Kenney, Denise J. Montell*

7

8

9 MCDB Department

10 University of California

11 Santa Barbara, CA 93106

12 *to whom correspondence should be addressed

13 **Abstract**

14 Adult stem cells commonly give rise to transit-amplifying progenitors, whose progeny differentiate into

15 distinct cell types. Signals within the stem cell niche maintain the undifferentiated state. However it is

16 unclear whether or how niche signals might also coordinate fate decisions within the progenitor pool.

17 Here we use quantitative microscopy to elucidate distinct roles for Wnt, Hedgehog (Hh), and Notch

18 signalling in progenitor development in the Drosophila ovary. Follicle stem cells (FSCs) self-renew and

19 produce precursors whose progeny adopt distinct polar, stalk, and main body cell fates. We show that a

20 steep gradient of Wnt signalling maintains a multipotent state in proximally located progenitor cells by

21 inhibiting expression of the cell fate determinant Eyes Absent (Eya). A shallower gradient of Hh

22 signalling controls the proliferation to differentiation transition. The combination of Notch and Wnt

23 signalling specifies polar cells. These findings reveal a mechanism by which multiple niche signals

24 coordinate cell fate diversification of progenitor cells.

Introduction

Adult stem cells are important for tissue homeostasis and regeneration due to their ability to both self-renew and generate multiple types of differentiated daughters. Adult stem cells are located in a niche that provides the proper microenvironment to maintain "stemness" [1,2]. The progeny of stem cells that move away from the niche generally go through a precursor cell (or progenitor cell, transit amplifying cell) stage before they differentiate [3,4]. However, it is unclear whether the precursor state is simply a loss of stemness due to displacement from niche signals, or whether secreted niche factors might act as morphogens that establish distinct cell fates at different concentrations and distances from the niche.

The Drosophila ovary is an appealing model for studying adult stem cells [5]. Each ovary contains 16-20 ovarioles, which are chains of egg chambers in increasing stages of maturity [6]. The anatomy thus displays the temporal sequence of ongoing developmental events (Fig. 1a). Development begins in the germarium, which is located at the anterior tip of the ovariole. The anterior half of the germarium, region 1, contains germline stem cells and their progeny, which continue dividing to produce 16-cell cysts. Somatic escort cells surround the developing cysts as they progress to region 2a. The FSCs are located at the region 2a/2b boundary [7], where germ cysts exchange their escort cell covering for the FSC daughters. The posterior half of the germarium contains flattened cysts in region 2b, followed by rounded region 3 cysts. Follicle precursor cells associate with region 2b and region 3 cysts, and their progeny adopt distinct polar, stalk, and main body cell fates, which serve different functions in normal egg chamber development. However the molecular mechanisms that govern these earliest cell fate decisions are unknown and most precursors in region 2b and region 3 do not yet express mature cell fate markers [8–10].

Several signalling pathways have been implicated in regulating follicle precursor cell fate specification and differentiation. Notch signalling is required for polar cell specification [9] and is

3

50   present in mature polar cells at high levels in stage 1 [11]. Earlier Notch activity at the region 2a/2b

51   boundary is required for the migration of one FSC daughter laterally across the germarium, while

52   other daughters move posteriorly [8]. However, Notch activity does not seem to be sufficient to

53   induce ectopic polar cells in the main body region [10], raising the question whether additional

54   factors are required for polar cell specification. Follicle stem and precursor cells receive signals

55   secreted from the niche escort cells, in addition to germline Delta, which activates the Notch

56   receptor on follicle cells. Niche factors including Wnt, Hh, epidermal growth factor, and bone

57   morphogenetic protein, which are crucial in many adult stem cell niches, are important for FSC

58   maintenance [12–18]. Hyper-activation of Wnt or Hh signalling causes defects in follicle cell

59   differentiation [12,19], but the origin of these phenotypes is not understood and it remains unclear

60   whether these niche signals normally regulate progenitor cell fate or differentiation.

61

62   In a forward genetic screen for mutations that disrupt cell fates in the ovary, we identified a mutant

63   allele of *Axin (Axn)*, a negative regulator in the Wnt pathway. Superficially, the phenotype resembled

64   that caused by mutations in *patched (ptc)* or *costal* (*cos*), two negative regulators of Hh signalling.

65   However, we traced both defects back to the earliest steps of follicle cell specification. We developed

66   quantitative analyses of the differentiation markers, Eya and Cas, as well as Wnt, Hh and Notch

67   signalling reporters to reveal distinct roles of these three pathways. We found that a Wnt signal from the

68   FSC niche maintains proximally located progenitor cells in a multipotent state by suppressing the cell

69   fate determinant Eya, whereas a graded Hh signal delays differentiation of all follicle cell types. Notch

70   coordinates with Wnt and Hh in both space and time to specify polar cells. The combination of these

71   three signals produces appropriate spatial patterning of cell types and temporal patterning of

72   differentiation.

73

4

74 **Results**

75 **Distinct effects of Wnt and Hh hyper-activation on follicle cell differentiation**

76 At stage 8 of oogenesis, anterior polar cells specify neighbouring epithelial follicle cells as motile border

77 cells, and together they migrate as a cluster during stage 9 (Fig. 1a). In a forward genetic screen of EMS-

78 induced mutations that cause border cell defects in mosaic clones [20], we identified a line that produced

79 abnormally large border cell clusters. Compared to control clusters, which are usually composed of 5-7

80 migratory cells surrounding two polar cells, clusters containing mutant cells showed as many as 6-12

81 polar cells and 14-35 total cells per cluster (Fig. 1b-d). The phenotype was autonomous to the polar

82 cells, as supernumerary polar cells and over-sized border cell clusters were only observed when polar

83 cells were homozygous for the mutation (Fig. 1d). The supernumerary polar cell phenotype resembled

84 those previously reported for *eya* [21], *cos* [22], and *ptc* (Fig. 1e; [19]). We mapped the new mutation to

85 genomic location 99D3 (Supplementary Fig. 1a-b), which contains the *Axn* gene. *Axn* allele S044230

86 produced a similar phenotype (Supplementary Fig. 2) and failed to complement the new mutation for

87 lethality. We therefore named the new allele *Axn^{1511}*. This supernumerary polar cell phenotype was

88 somewhat surprising as it had not previously been reported for the *Axn* gene.

89

90 In addition to supernumerary polar cells, *Axn$^-$* and *ptc$^-$* clones showed abnormal stalks, consistent with

91 previous reports [12,23]. Polar and stalk cell specification occurs early in the germarium, and these cells

92 stop dividing soon after they exit the germarium [7,24]. In the ovary, hyperactive Wnt or Hh signalling

93 affects differentiation [12,19]. We asked exactly what aspects of differentiation were affected by Wnt or Hh

94 hyper-activation.

95 We used two complementary markers, Eya [21] and Cas [25] (Fig. 2a). To be comprehensive, we performed

96 3D reconstructions of ovarioles and quantified the levels of both Eya and Cas in every somatic cell (Fig.

97 2b; Supplementary Fig. 3). We found barely detectable levels of either protein in regions 1 and 2a escort

5

98   cells. Low but increasing levels of both Eya and Cas were present in FSCs and their immediate

99   daughters in region 2b^A and 2b^P. Eya and Cas show differential expression in region 3/stage 1, such that

100   some cells expressed higher levels of one or the other (indicated by divergence from the diagonal in the

101   graphs in Fig. 2b). As development proceeded through stages 1-4, the levels of Eya and Cas diverged

102   more and more. By stage 4, Eya and Cas became completely distinct markers for main body (Eya$^+$ Cas$^-$)

103   versus polar/stalk (Eya$^-$ Cas$^+$) fates (Fig. 2a-b). Thus, Eya and Cas are excellent markers for studying the

104   earliest cell fate diversification in the ovary.

105   To examine the differentiation defect caused by hyperactive Wnt or Hh signalling, we made FSC clones

106   and stained them for Eya and Cas (Fig. 2c-d). Hyperactive Wnt signalling by loss of the β-catenin [or

107   Armadillo (Arm) in Drosophila] destruction complex component *Axn*$^-$ or *adenomatous polyposis coli*

108   (*Apc*$^-$) produced many egg chambers containing only Eya$^-$ Cas$^+$, polar/stalk-like mutant cells, in contrast

109   to control clones in which Eya$^+$ cells were frequent (Fig. 2c,e). In contrast, FSC clone with hyperactive

110   Hh signalling by loss of the negative regulators *ptc*$^-$ or *cos*$^-$ were not biased toward polar/stalk fates.

111   They instead produced many Eya$^+$ Cas$^+$ cells in stage 4 that resembled control cells in stage 1-2. Eya$^+$

112   Cas$^+$ cells were virtually never observed in controls in stage 4 (Fig. 2b,d,f). These results suggested

113   distinct differentiation problems in Wnt or Hh hyper-activation, and prompted us to examine their cause

114   and the endogenous function of Wnt and Hh in further detail.

115

116   **Wnt and Hh act independently in the germarium**

117   Wnt and Hh signalling positively regulate one another in some settings [26], while they antagonize [27,28] or

118   play independent roles in other cases [29]. In the ovary, Wnt and Hh are stem cell niche factors produced

119   in cap cells and escort cells [16–18,30]. To understand their relationship, we examined Wnt and Hh activity

120   patterns. We used *frizzled 3* (*fz3*)-*RFP* [31,32], which is a reporter for Wnt signalling activity, in order to

121   assess the pattern of Wnt pathway activation. *fz3-RFP* was highly expressed in region 1-2a and showed

122   a graded pattern in region 2b (Fig. 3a-b). The *fz3-RFP* signal was reduced in *armRNAi* expressing clones

6

123   and increased in *Axn*[-] clones, demonstrating that it is indeed responsive to Wnt signalling (Fig. 3c-d;

124   Supplementary Fig. 4a). *ptc-GFP* is a reporter for Hh signalling [18] and shows a pattern similar to *fz3-*

125   *RFP* (Fig. 3e-f), though the gradient appears to extend more posteriorly. The *ptc-GFP* signal was

126   reduced when knocking down *smoothened* (*smo*), a positive regulator in the Hh pathway (Fig. 3g-h;

127   Supplementary Fig. 4b). Unexpectedly, *cosRNAi* also caused a reduction of *ptc-GFP* signal in region 2b

128   (Fig. 3g-h; Supplementary Fig. 4c), while in later stages the signal increased as expected for loss of a

129   negative regulator (Supplementary Fig. 5). To decipher the relationship between Wnt and Hh signalling

130   in the germarium, we examined the pattern of *fz3-RFP* in *smo*[-] or *ptc*[-] clones and the pattern of *ptc-GFP*

131   in *dishevelled* (*dsh*, a positive regulator in the Wnt pathway) or *Axn* mutant clones. Changing Hh

132   signalling had no detectable effect on the Wnt activity pattern in region 2b (Fig. 3c-d), nor did changing

133   Wnt signalling influence Hh activity (Fig. 3g-h). Thus, Wnt and Hh appear to function independently in

134   the ovary.

135

136   **Wnt signalling inhibits expression of the main body fate determinant Eya**

137   *Axn*[-] FSC clones frequently gave rise exclusively to Cas^{+} cells (Fig. 4a-b). *Axn*[-] clones appear in the

138   normal polar/stalk region, or as small clones in the main body region forming ectopic polar and stalk

139   cells, or as large clones that form a continuous stalk with a single polar cell cluster, causing the egg

140   chamber to appear to bud from the side. Clones generated at a later stage, however, did not show this

141   cell fate bias (Supplementary Fig. 6; [12]), suggesting a narrow developmental time window for Wnt

142   signalling to affect cell fate. To understand how hyper-activation of Wnt created clones biased toward

143   Cas[+] polar/stalk-like fate, we considered a few possibilities. The *Axn*[-] Eya[+] main body precursors may

144   not survive, or Cas[+] polar/stalk-like cells may proliferate more. Alternatively or in addition, more cells

145   may adopt a polar/stalk-like fate than a main body fate.

146   During early stages of oogenesis, apoptosis was common in polar and stalk cells but rare in main body

147   cells (Fig. 4c). *Axn*[-] clones in region 3-stage 2 main body regions did not show a detectable increase in

7

148　apoptosis (Fig. 4c). The mitotic marker EdU was not detected in control stalk regions after stage 2, but

149　was detected in Axn^- Cas^+ cells (Fig. 4d), suggesting that these polar/stalk-like cells proliferate more.

150　Strikingly, we found a decrease of Eya and increase of Cas in the main body region in Axn^- cells as early

151　as region 3, suggesting a shift in cell fate (Fig. 4e-f). Such small clones in the main body region likely

152　gave rise to ectopic Eya^- Cas^+ clones observed in stage 4 egg chambers, whereas large main body region

153　clones likely developed into continuous stalks with a single polar cell cluster, causing the egg chamber

154　to appear to bud from the side (Fig. 4a).

155　To understand how Wnt signalling affects follicle precursor cell differentiation, we quantified the

156　change in Eya and Cas levels in the germarium region 2b. Eya was significantly reduced in the Axn^-

157　clones (Fig. 4g). Conversely, dsh^- cells showed significantly increased Eya in region 2b (Fig. 4g),

158　suggesting that Wnt signalling normally functions to inhibit Eya expression. Reducing Wnt signalling by

159　expressing $armRNAi$ in the Axn^- clone also resulted in increase of Eya, relative to control. Cas was also

160　reduced in Axn^- cells in region 2b, but to a lesser degree than Eya, which was also observed upon eya

161　knockdown in this region (Fig. 4g).

162　Knocking down eya in mosaic clones caused all mutant cells to become Eya^- Cas^+, which phenocopied

163　Axn^- (Fig. 4h). To test how important the reduction of Eya is for the fate change in Axn^- cells, we

164　expressed UAS-eya in Axn^- clones. Indeed Eya expression restored main body cell fate (Fig. 4h;

165　Supplementary Fig. 7). Therefore Eya is a key target of Wnt signalling. Expression of Eya in Axn^- clones

166　also produced Eya^+ Cas^+ cells and Cas^+ Eya^- cells, which were observed when expressing UAS-eya alone

167　in mosaic clones. This was likely due to variations in the timing and level of Eya expressions in these

168　experiments, which were not possible to control precisely. These results show that the primary effect of

169　Wnt signalling is to suppress expression of the main body cell fate determinant Eya.

170

171　**Notch activity in the germarium promotes polar cell specification**

8

172   Our results indicate that Wnt signalling enables polar and stalk fates by keeping the Eya level low

173   in the region proximal to the FSC niche, raising the question as to how Wnt relates to Notch in

174   specifying polar cell fate. We used a Notch activity reporter, the *Notch responsive element* (*NRE*)

175   fused green fluorescent proteins [33] to address this question. NRE-GFP showed a basal level in all

176   cells, but peaked in a subset of cap cells, in region 2a/2b boundary cells, and in polar cells (Fig. 5a-

177   b). This is consistent with the roles of Notch in the germline stem cell niche [34,35], cross-migration

178   of FSC daughters [8], and polar cell specification [9,36]. *Axn⁻* clones showed high Notch activity in polar

179   cells both at normal and ectopic locations that were directly contacting germline, suggesting that a

180   high Wnt signalling predisposes cells to specification as polar cells by Notch (Fig. 5c).

181   To assess the effect of Notch signalling on follicle precursor development in the germarium, we

182   quantified the Eya and Cas levels in *NotchRNAi* FSC clones. Reduction of Notch decreased Cas and

183   increased Eya in region 2b as well as the proximal region of stage 1 (Fig. 5d; Supplementary Fig.

184   8). This is in agreement with the role of Notch in polar cell specification and indeed, we observed

185   high frequency of fused egg chambers when the clone covered the anterior polar cell region.

186   Therefore, Wnt enables polar and stalk fates primarily by suppressing premature Eya expression,

187   whereas Notch promotes polar cell specification and affects both Cas and Eya.

188

189   **Hh signalling controls the timing of proliferation versus differentiation**

190   Hyperactive Hh signalling delayed differentiation as shown by the expression pattern of Eya and Cas in

191   stage 4 and later (Fig. 2b,d,f; Supplementary Fig. 9a), as well as expression of the stalk cell marker

192   lamin C (Fig. 6a; [12]) and the polar cell marker NRE-GFP (Supplementary Fig. 9b), consistent with

193   earlier reports using different markers [19,30]. How does delayed differentiation change the pattern of

194   follicle cell fates and cause both excess (Fig. 1e; Fig. 6a) and ectopic (Fig. 2d; Supplementary Fig. 9a;

195   [30,37]) polar/stalk-like cells?

9

196   We first analysed the long stalk phenotype. The supernumerary stalk cell phenotype appeared most

197   obvious when the majority of follicle cells associated with an egg chamber were mutant. In contrast to

198   control stalks that contained a stable number of stalk cells ranging from 6-13, ptc^- stalks contained an

199   average of 21 cells at stage 2, and continued to increase in number over time (Fig. 6a-b). Another feature

200   of stalk cell maturation is that they normally become physically separated from the polar cells (Fig. 6a,

201   arrowhead), even though stalk cells initially form in the polar region (Fig. 6a, arrow). In contrast, ptc^-

202   stalk cells remained associated with the poles, and with Cas^+ or lamin C^+ positive cells on the main body

203   follicle layer (Fig. 6a, arrow). Mature stalk cells with high Cas were normally not proliferative, and thus

204   were EdU-negative after stage 2 (Fig. 6c). In ovarioles with ptc^- clones in regions where stalk was still

205   connected to polar and/or main body cells, Eya and Cas continued to be co-expressed (Fig. 6d),

206   suggesting that they are multipotent precursors. These cells were EdU positive (Fig. 6c). Therefore, we

207   conclude that excessive stalk cell production in ptc^- is due to persistence of precursor cells that

208   contribute cells to the enlarging stalk.

209   We then asked how supernumerary polar cells form in response to Hh hyper-activation. Typically 3-6

210   polar cells form and all but two are eliminated by apoptosis [38], a process that requires JAK/STAT

211   signalling [39]. We observed a reduction of JAK/STAT activation in mutant polar cell regions (Fig. 6e),

212   likely caused by the differentiation delay, which also delayed Upd production. There was also reduced

213   apoptosis in the polar cells (Fig. 6f). Therefore, the excess polar cells appeared to result from delayed

214   differentiation, which also postponed apoptosis.

215   Furthermore, some ptc^- cells in the main body region adopted a polar or stalk cell fate as they matured

216   (Supplementary Fig. 6a), and thus formed ectopic polar/stalk cells. In this situation $Eya^+ Cas^+$

217   precursors, present due to the developmental delay, differentiated later than normal and thus in the

218   absence of proper spatial patterning signals (see discussion).

219   If hyperactive Hh signalling delays differentiation, would loss of Hh signalling expedite differentiation?

220   Earlier studies have not detected a defect in differentiation in smo^- [19], but these studies did not have

10

221   access to early cell fate markers and quantitative imaging. Using our quantitative analysis of Eya and

222   Cas in the germarium, we observed significantly higher Cas expression in smo^- cells in region 2b (Fig.

223   6g). We also observed premature differentiation of polar cells using *NRE-RFP* (Fig. 6h), which was

224   never seen in controls at the same stage. The smo^- clone size was significantly smaller than ptc^- or

225   control, suggesting premature termination of proliferation (Fig. 6i).

226

227   **Wnt and Hh double mutants show additive effects on egg chamber patterning**

228   Since Wnt and Hh show independent activities and have distinct functions in follicle precursor cell

229   differentiation, we hypothesized that combined loss of Wnt and Hh activity should show a more extreme

230   egg chamber formation phenotype than either alone. We used C306-Gal4 to drive *smo* and *dsh* RNAi in

231   the follicle precursor cells (Supplementary Fig. 10a). Indeed, we observed an increase in the frequency

232   of egg chamber fusions to 80% in double RNAi knockdowns compared to 30-40% for the single

233   knockdowns (Fig. 7a; Supplementary Fig. 10b), a defect indicating a problem with producing the correct

234   number of polar and stalk cells in the right location for egg chamber budding.

235   We further predicted that hyper-activation of both Wnt and Hh would show an additive effect. Indeed,

236   whereas there are normally 8-10 stalk cells, we observed an average of 30 stalk cells in *Axn* or *cos* single

237   mutant, and a number that doubled following Wnt and Hh double hyper-activation (Fig. 7b;

238   Supplementary Fig. 11). The *Axn* or *cos* double mutant cells are still largely biased toward Cas$^+$

239   polar/stalk like cells (Fig. 7c), suggesting that the Eya$^+$ Cas$^+$ precursors that accumulated due to delayed

240   differentiation preferentially adopted a polar/stalk fate in the presence of high Wnt signalling.

241

242   **Discussion**

243   When adult tissue stem cells divide asymmetrically to self-renew and produce a daughter cell that

244   commonly becomes a transit amplifying precursor, one possibility is that the stem cell retains its

245   character by virtue of its association and proximity to niche signals whereas the transient amplifying

246   precursor acquires its properties due to displacement from the niche. Here we use the Drosophila ovary

247   model to address the roles of secreted niche factors in diversification of precursor cell fates as they leave

248   the niche. We found that Wnt and Hh act as morphogens that not only maintain FSC at a high

249   concentration, but also provide critical instructions for the development of the transit amplifying follicle

250   precursor population at a lower concentration. The distinct shapes of the gradients of these niche signals

251   serve important functions. A key finding is that Wnt signals maintain multipotency in a subset of

252   precursors that maintain closer proximity to the niche, whereas reduced Wnt signalling activates Eya

253   expression in precursors displaced further from the niche and this restricts them to the main body cell

254   fate.

255   Earlier studies reported egg chamber formation defects due to reducing the Wnt or Hh ligand levels

256   [12,18,30]. However, recent studies found roles of Wnt and Hh in escort cells to affect germline

257   differentiation [16,17,40,41], therefore the ovariole defects from reduction of Wnt or Hh ligands could either

258   be caused by effects on the germline and/or follicle cells. We clarified this issue by reducing Wnt and

259   Hh intracellular signalling components directly in follicle cells in mosaic clones, or by RNAi

260   knockdown specifically in follicle precursor cells.

261   In the germarium, the follicle precursor cells in region 2b and region 3 contain both specified and

262   unspecified cells [8], yet previous studies lacked cell fate markers and quantitative methods to assess the

263   influence of different signalling inputs. Our quantitative analysis of the Wnt, Hh and Notch signalling

264   reporters as well as the differentiation factors, Eya and Cas, not only provide a sensitive and detailed

265   description of the FSC differentiation process, but also reveal early changes in the germarium that were

266   not previously detected. First, reduction of Wnt activity by *dsh⁻* or *armRNAi* increased the expression of

267   Eya, a key main body fate determinant [21], and reduction of Wnt by *C306-Gal4* driven *dshRNAi* in large

268   numbers of precursor cells caused egg chamber fusing, a phenotype also seen when driving *UAS-eya* by

269   *C306-Gal4* [25]. Second, reduction of Hh activity by *smo⁻* resulted in increased levels of Cas in region 2b,

270   indicative of premature differentiation. However, the Eya level did not increase in region 2b, which is

12

271 likely because of inhibition of Eya by Wnt in this region. Third, reduction of Notch activity shifted the

272 balance between Eya and Cas in region 2b.

273 Our results suggest an integrated model for how Wnt and Hh stem cell niche signals act in coordination

274 with the differentiation factor Notch to establish the initial asymmetry and specify cell fates during

275 follicle precursor cell differentiation in the germarium (Fig. 7d). We propose that follicle precursor cells

276 expressing low levels of Cas and Eya have intrinsically unstable fates that can stochastically give rise to

277 $Eya^+ Cas^+$, $Eya^+ Cas^-$, or $Eya^- Cas^+$ cells in the absence of specific instructive signals. The spatial

278 patterns of Wnt, Hh and Notch function as environmental cues to direct these precursor cells to produce

279 the appropriate numbers and types of differentiated cells.

280 We show that hyper-activation of Wnt signalling biases follicle cells to polar and stalk cell fates, both of

281 which lack Eya and express high levels of Cas. A simple interpretation of these results might suggest

282 that the follicle precursor cells that retain higher Wnt signalling adopt a polar/stalk precursor fate

283 whereas the ones further displaced from the niche with disinhibited Eya adopt the main body precursor

284 fate. However there are clear data demonstrating that there is no dedicated polar/stalk precursor [8], while

285 the same clonal analyses are perfectly consistent with the existence of a dedicated main body precursor

286 cell. Therefore we propose that the steep gradient of Wnt in region 2b results in progenitor cells with

287 different levels of Wnt signalling. The progenitor cells that are displaced from the niche, the posterior

288 daughter of the FSC, escape Wnt signalling and therefore express Eya and adopt a dedicated main body

289 precursor fate. The progenitors that remain closer to the niche, the cross migrating cell and its daughter,

290 receive more Wnt ligand [16,17] and thus maintain a pluripotent state that is permissive for polar and stalk

291 fates but not irreversibly committed to those fates. Both the absolute and relative levels of Eya and Cas

292 are likely to be important for the final fate.

293 The Hh gradient in the germarium provides important temporal information to be coupled with the

294 spatial information as developing cysts move posteriorly and away from the FSC niche. In the absence

295 of proper coordination of differentiation and fate, cells can acquire random fates, as observed in stage 4

13

296   *ptc* or *cos* mutant clones for example (Fig. 2d, f). These cells lack the spatial patterning normally

297   provided by Wnt signalling by the time they differentiate. When Wnt and Hh signalling are co-activated,

298   most of the cells adopt polar/stalk-like fate (Fig. 7c).

299   Notch specifies polar cells through two actions in the germarium. First, Notch activity affects expression

300   of Eya and Cas in region 2b, likely indirectly by promoting the cross migration of FSC daughters [8] so

301   the precursor cells remain in high Wnt for longer. As a result, cells with reduced Notch activity in region

302   2b preferentially undergo posterior rather than lateral migration, and therefore escape from Wnt sooner

303   and express higher Eya. Meanwhile, the reduction of Cas in Notch mutant cells is likely because they

304   differentiate slower and therefore escape from Hh later, similar to the Notch and Hh antagonism

305   described in the mitosis to endocycle switch [42]. Second, relatively higher Notch activity due to germline

306   contact [43] and fringe expression [44] specify polar cells from the Eya^{low} multipotent precursor cell pool.

307   Although essential for polar cell specification, hyper-activation of Notch does not seem sufficient for

308   polar cell formation since excess polar cells only form in the two poles rather than on the main body

309   region [10], This implies that additional spatial information is required besides Notch activity for polar cell

310   formation. Here we found that spatial information to be a short-range Wnt signalling. Notch activity

311   coordinates with Wnt to specify polar cells.

312   Wnt, Hh and Notch are common players in many adult stem cell systems including the skin, gut, and

313   blood [45–47], which all possess a transit-amplifying progenitor pool close to the stem cell niche. Our

314   finding of the distinct functions of Wnt, Hh, and Notch in precursor cell fate specification provides an

315   integrated model for how multiple signalling inputs establish the initial asymmetry in cell fates. The

316   additive effect of hyper-activation of multiple signalling pathways that we observed may have

317   implications in cancer stem cell and its targeted treatment [48].

318

319   **Methods**

320   **Drosophila genetics and mosaic clone induction**

14

321   Fly strains used in this study are listed in Supplementary Table 1. Fly genotypes used in each experiment

322   are listed in Supplementary Table 2. Stocks were maintained at room temperature. Crosses were initiated

323   at room temperature and transferred to 25 °C at 2-3 instar larvae stage. For C306Gal4; tubGal80ts

324   experiments, adult female flies were transferred to 29 °C for 7-10 days after eclosion. Egg chamber

325   stage was determined based on germ cell nucleus diameter listed in Supplementary Table 3.

326

327   Mosaic clones were generated using the FLP/FRT system. 8-9 newly eclosed adult female flies (1-2

328   days old) along with 8 males were collected in a vial with wet yeast paste (dry yeast and water 1:1.5)

329   and dry yeast and kept at 25 °C. Flies were flipped without CO_2 to a fresh vial daily until dissection, and

330   heat shocked 2 days after collection. Males were added if less than 3 were present to ensure optimal

331   ovary development. For making FSC clones up to stage 5, flies were heat shocked twice for 1 hour,

332   about 4 hours apart, in a 37 °C water bath, and then were kept at 25 °C for 5-7 days before dissection.

333   For RNAi knockdown experiments, flies were transferred to 29 °C after heat shock (except for *eyaRNAi*

334   and *armRNAi,* which were kept at 25 °C). For making FSC clones up to stage 8, flies were kept for 6-8

335   days before dissection. For border cell clones in Fig. 1d, flies were heat shocked once for 30 minutes

336   and kept for 4-5 days before dissection. For MARCM clones, we observed some leaky GFP expression

337   in follicle cells in stage 6 and later, likely due to actinGal4 being too strong in stage 6 and later such that

338   tubGal80 was not able to suppress all Gal4 activities. Therefore, we only analysed MARCM clones

339   before stage 6.

340

341   **Immunostaining and EdU incorporation**

342   Adult female ovaries were dissected in Schneider's *Drosophila* medium (Thermo Fisher Scientific,

343   Waltham, MA) with 20% fetal bovine serum and transferred to a 0.6 ml microfuge tube with 100 μl

344   dissection medium. Ovaries were dissociated by pipetting up and down approximately 50 times using a

345   200 μl pipette set to 50 μl. Dissociation in this way causes random physical damage to the egg chambers

15

346   [49], but we found it more efficient than pulling ovarioles out of the muscle sheath using forceps, which

347   causes more damage to the germarium or younger egg chambers. Ovarioles were immediately fixed for

348   20 minutes in 4% paraformaldehyde at 4 °C. After fixation, ovarioles were washed with PBS/0.4%

349   Triton X-100 (PBST), and then incubated with primary antibodies overnight at 4 °C. The following day,

350   ovarioles were washed with PBST before incubation in secondary antibody for 1.5-2 hours. After

351   removal of secondary antibodies, samples were stained with Hoechst for 20 minutes. Samples were

352   washed in PBST before sorting in PBST. Sorting was conducted by using forceps under a dissection

353   microscope to remove mature eggs and clustered ovarioles from a given sample for optimal mounting.

354   Without sorting, mature eggs make it difficult to compress the sample, the germaria can be tilted,

355   whereas clustered ovarioles often overlap each other rendering imaging difficult. After sorting, samples

356   were stored in VECTASHIELD (Vector Laboratories, Burlingame, CA) at 4 °C.

357   The following antibodies were used in this study: chicken anti-GFP (1:2000, Abcam, Cambridge, UK;

358   13970) (used to amplify MARCM GFP, Flipout GFP, Ptc-pelican-GFP, and NRE-GFP, not used on

359   negative mosaic ubi-GFPnls), rabbit anti-dsRed (1:1000, Takara Bio USA, Mountain View, CA;

360   632496) (used to amplify Flipout RFP and NRE-RFP, not used on negative mosaic ubi-RFPnls or Fz3-

361   RFP), mouse anti-Eyes Absent [1:50-200, Developmental Studies Hybridoma Bank (DSHB), Iowa City,

362   IA; 10H6, needs pre-absorption if staining is noisy], mouse anti-Fascillin III (1:50, DSHB 7G10), rat

363   anti-E-cadherin (1:50, DSHB DCAD2), rabbit anti-Castor [1:5000, Ward F. Odenwald, [50]], mouse anti-

364   Armadillo (1:100, DSHB N27A1), mouse anti-Smoothened (1:4, DSHB 20C6), rat anti-Cubitus

365   interruptus (1:10, DSHB 2A1), rabbit anti-cleaved Drosophila caspase 1 (1:200, Cell Signaling

366   Technology, Danvers, MA; 9578), mouse anti-Notch intracellular domain (1:200, DSHB C17.9C6), and

367   mouse anti-Lamin C (1:200, DSHB LC28.26).

368   For 5-ethynyl-2'-deoxyuridine (EdU) incorporation, adult female ovaries were dissected in Schneider's

369   *Drosophila* medium with 20% fetal bovine serum and transferred to a microfuge tube with the dissection

370   medium plus 40 μM EdU, and kept at room temperature on a shaker for 1 hour. Ovarioles were then

16

371   dissociated, fixed, and stained with primary and secondary antibodies as described above. Before

372   staining with Hoechst, an EdU detection reaction was performed according to the manufacturer's

373   manual (Thermo Fisher Scientific).

374

375   **Imaging and image processing**

376   Due to the spherical organization of the egg chambers, few follicle cells have their nuclei located on the

377   same imaging focal plane. Therefore, we imaged the egg chambers in full Z stacks. Samples were

378   mounted on a glass slide in VECTASHIELD (25 μl for early stage ovarioles, or 65 μl for stage 9/10)

379   using a 22 mm X 40 mm cover glass, to ensure that the germarium was mounted flat, but not

380   compressed, and that later stages were compressed to a consistent degree. All images were taken on a

381   Zeiss LSM780 confocal microscope, using a 40x 1.4 N.A. oil objective. Z stacks covering the entire

382   germaria or ovarioles were taken with a 0.43 μm step size for germarium and ovarioles, or a 1 μm step

383   size for border cell clusters. XY resolution is 0.14 μm for germaria, or 0.35 μm for ovarioles. Laser

384   power corrections were applied by increasing the laser power as the objective scans from the top of the

385   sample to the bottom of the sample, so that the signal on the bottom did not appear weaker than the top.

386   3D images were visualized in Imaris (Bitplane, South Windsor, CT), and annotated in Excel (Microsoft,

387   Redmond, WA), to categorize the developmental stage, sample condition, mounting condition, imaging

388   condition, clone location, and result interpretation. Developmental stage was determined as described

389   above. Sample condition includes whether they were damaged, or still tightly packed in muscle sheath.

390   Severely damaged egg chambers had an incomplete follicle epithelium and leaky germ cells, or large

391   patches of follicle cells without nuclear stain. Mild damage caused a small patch of follicle cells to show

392   condensed Hoechst staining, and diffused or reduced nuclei Eya, Cas, or ubi-GFP/RFPnls signal [49].

393   Samples with severe damage were not analysed, and the damaged cells in a sample with mild damage

394   were not included in the analysis. We preferred to analyse samples out of the muscle sheath, because

395   their morphology was not affected by squeezing from neighbouring egg chambers. Samples tightly

17

396   packed in muscle sheath were not used for intensity measurement because it was difficult to perform

397   laser power correction. Mounting condition denotes if the sample was too compressed or too tilted. If the

398   germarium was too compressed, the germline cysts were squeezed and it was difficult to perform 3D

399   rotation as described below. If too tilted, laser correction became difficult. Imaging condition marks

400   whether the image was taken with proper laser power correction. This was estimated by comparing the

401   signal intensity of the top, middle, and bottom of the sample visually, and was quantified as described

402   below. Clone location and result interpretation were listed to help summarize the results, draw

403   conclusions based on the phenotype seen across multiple ovarioles, and select representative images for

404   presentation.

405   Representative images were exported from Imaris using either Easy 3D view or slice view. Since

406   different follicle cell nuclei were located on different focal planes, 2-5 μm Z stacks were used to show

407   single follicle cell layers, while 12-25 μm Z stacks were used to show one half of the egg chambers.

408   Exported images were rotated and cropped in Photoshop (Adobe, San Jose, CA). Single channel images

409   were converted from a black background to a white background using Invert LUT function in Fiji [51].

410

411   **3D quantification**

412   Image segmentation was performed using Imaris. First, samples were rotated using the Free Rotate

413   function. Egg chambers were rotated so the polar cells aligned horizontally, with the anterior to the left.

414   Germaria were rotated in two steps. The first step positioned region 2b cysts vertically in the Z-direction

415   by placing an Oblique Slicer in the mid-sagittal section of the germaria, and performing free rotation to

416   the orthogonal view of the oblique slicer. The second step rotated the germaria anterior to the left to

417   place region 2b cysts vertically in XY-direction. Second, follicle cell nuclei were detected using the

418   Spots function. For the germaria, a 2.5 μm diameter spot size was used for automatic spot detection in

419   the channel with follicle cell nuclei signals. Spots were then manually edited so that each follicle cell

420   was marked. Dividing, dying, or damaged cells showed clear signs, including condensed Hoechst

18

421   staining and diffused, or reduced, nuclei Eya, Cas, or ubi-GFP/RFP signal, and were not quantified. The

422   2.5 μm spots were then used to create a masked channel, and automatic spots detection based on that

423   channel was applied to create 1.75 μm spots, so that only the center of the nuclei with a strong and even

424   signal was used for quantification. For egg chambers, a 3.46 μm diameter spot size was used for

425   automatic spot detection, followed by reduction to 1.75-2 μm. Third, background intensities were

426   estimated by placing 8-12 1.75-2 μm spots in two Z planes in same region as the measured follicle cells.

427   For Eya and Cas, background spots were placed in the germ cell cytoplasm, while for Wnt or Hh

428   reporters they were placed in the region 2b germ cell nuclei. Fourth, accuracy of laser power correction

429   was determined by selecting control cells at the top, middle, and bottom of the germarium or egg

430   chamber in the same region, and comparing their signal intensities.

431   Data for spot position and channel mean intensity were exported from Imaris, and processed using

432   MATLAB (MathWorks, Natick, MA) for background subtraction, comparison of top, middle, and

433   bottom intensity, and normalization, and plotted using Prism (GraphPad, La Jolla, CA).

434

435   **Statistics**

436   Statistics were performed using Prism. Unpaired t-test was used for comparing two groups, and

437   Ordinary one-way ANOVA, followed by Tukey's multiple comparisons test, was used for comparing

438   multiple groups. For box plots, the Tukey method was used for plotting whiskers and outliers.

19

References

440 1. Xie, T. & Spradling, A. C. A niche maintaining germ line stem cells in the Drosophila ovary.
441   Science **290,** 328–330 (2000).
442 2. Song, X. & Xie, T. DE-cadherin-mediated cell adhesion is essential for maintaining somatic stem
443   cells in the Drosophila ovary. Proc Natl Acad Sci U S A **99,** 14813–14818 (2002).
444 3. Mascré, G. et al. Distinct contribution of stem and progenitor cells to epidermal maintenance.
445   Nature **489,** 257–262 (2012).
446 4. Hsu, Y. C., Li, L. & Fuchs, E. Transit-amplifying cells orchestrate stem cell activity and tissue
447   regeneration. Cell **157,** 935–949 (2014).
448 5. Losick, V. P., Morris, L. X., Fox, D. T. & Spradling, A. Drosophila stem cell niches: a decade of
449   discovery suggests a unified view of stem cell regulation. Dev Cell **21,** 159–171 (2011).
450 6. Spradling, A. C. in The development of Drosophila melanogaster 1–70 (Cold Spring Harbor
451   Laboratory Press, 1993).
452 7. Margolis, J. & Spradling, A. Identification and behavior of epithelial stem cells in the Drosophila
453   ovary. Development **121,** 3797–3807 (1995).
454 8. Nystul, T. & Spradling, A. Regulation of epithelial stem cell replacement and follicle formation in
455   the Drosophila ovary. Genetics **184,** 503–515 (2010).
456 9. Torres, I. L., López-Schier, H. & St Johnston, D. A Notch/Delta-dependent relay mechanism
457   establishes anterior-posterior polarity in Drosophila. Dev Cell **5,** 547–558 (2003).
458 10. Larkin, M. K., Holder, K., Yost, C., Giniger, E. & Ruohola-Baker, H. Expression of constitutively
459   active Notch arrests follicle cells at a precursor stage during Drosophila oogenesis and disrupts the
460   anterior-posterior axis of the oocyte. Development **122,** 3639–3650 (1996).
461 11. Assa-Kunik, E., Torres, I. L., Schejter, E. D., Johnston, D. S. & Shilo, B. Z. Drosophila follicle cells
462   are patterned by multiple levels of Notch signaling and antagonism between the Notch and
463   JAK/STAT pathways. Development **134,** 1161–1169 (2007).
464 12. Song, X. & Xie, T. Wingless signaling regulates the maintenance of ovarian somatic stem cells in
465   Drosophila. Development **130,** 3259–3268 (2003).
466 13. Zhang, Y. & Kalderon, D. Hedgehog acts as a somatic stem cell factor in the Drosophila ovary.
467   Nature **410,** 599–604 (2001).
468 14. Castanieto, A., Johnston, M. J. & Nystul, T. G. EGFR signaling promotes self-renewal through the
469   establishment of cell polarity in Drosophila follicle stem cells. elife **3,** (2014).
470 15. Kirilly, D., Spana, E. P., Perrimon, N., Padgett, R. W. & Xie, T. BMP signaling is required for
471   controlling somatic stem cell self-renewal in the Drosophila ovary. Dev Cell **9,** 651–662 (2005).
472 16. Wang, S. et al. Wnt signaling-mediated redox regulation maintains the germ line stem cell
473   differentiation niche. elife **4,** e08174 (2015).
474 17. Luo, L., Wang, H., Fan, C., Liu, S. & Cai, Y. Wnt ligands regulate Tkv expression to constrain Dpp
475   activity in the Drosophila ovarian stem cell niche. J Cell Biol **209,** 595–608 (2015).
476 18. Sahai-Hernandez, P. & Nystul, T. G. A dynamic population of stromal cells contributes to the
477   follicle stem cell niche in the Drosophila ovary. Development **140,** 4490–4498 (2013).
478 19. Zhang, Y. & Kalderon, D. Regulation of cell proliferation and patterning in Drosophila oogenesis
479   by Hedgehog signaling. Development **127,** 2165–2176 (2000).
480 20. Silver, D. L. & Montell, D. J. Paracrine signaling through the JAK/STAT pathway activates
481   invasive behavior of ovarian epithelial cells in Drosophila. Cell **107,** 831–841 (2001).
482 21. Bai, J. & Montell, D. Eyes absent, a key repressor of polar cell fate during Drosophila oogenesis.
483   Development **129,** 5377–5388 (2002).
484 22. Liu, Y. & Montell, D. J. Identification of mutations that cause cell migration defects in mosaic
485   clones. Development **126,** 1869–1878 (1999).

23. *Forbes, A. J., Spradling, A. C., Ingham, P. W. & Lin, H. The role of segment polarity genes during early oogenesis in Drosophila. Development* **122,** *3283–3294 (1996).*

24. *Tworoger, M., Larkin, M. K., Bryant, Z. & Ruohola-Baker, H. Mosaic analysis in the drosophila ovary reveals a common hedgehog-inducible precursor stage for stalk and polar cells. Genetics* **151,** *739–748 (1999).*

25. *Chang, Y. C., Jang, A. C., Lin, C. H. & Montell, D. J. Castor is required for Hedgehog-dependent cell-fate specification and follicle stem cell maintenance in Drosophila oogenesis. Proc Natl Acad Sci U S A* **110,** *E1734–42 (2013).*

26. *DiNardo, S., Heemskerk, J., Dougan, S. & O'Farrell, P. H. The making of a maggot: patterning the Drosophila embryonic epidermis. Curr Opin Genet Dev* **4,** *529–534 (1994).*

27. *Marcelle, C., Stark, M. R. & Bronner-Fraser, M. Coordinate actions of BMPs, Wnts, Shh and noggin mediate patterning of the dorsal somite. Development* **124,** *3955–3963 (1997).*

28. *Ouspenskaia, T., Matos, I., Mertz, A. F., Fiore, V. F. & Fuchs, E. WNT-SHH Antagonism Specifies and Expands Stem Cells prior to Niche Formation. Cell* **164,** *156–169 (2016).*

29. *Danesin, C. et al. Integration of telencephalic Wnt and hedgehog signaling center activities by Foxg1. Dev Cell* **16,** *576–587 (2009).*

30. *Forbes, A. J., Lin, H., Ingham, P. W. & Spradling, A. C. hedgehog is required for the proliferation and specification of ovarian somatic cells prior to egg chamber formation in Drosophila. Development* **122,** *1125–1135 (1996).*

31. *Olson, E. R. et al. Yan, an ETS-domain transcription factor, negatively modulates the Wingless pathway in the Drosophila eye. EMBO Rep* **12,** *1047–1054 (2011).*

32. *Wang, X. & Page-McCaw, A. A matrix metalloproteinase mediates long-distance attenuation of stem cell proliferation. J Cell Biol* **206,** *923–936 (2014).*

33. *Housden, B. E., Millen, K. & Bray, S. J. Drosophila Reporter Vectors Compatible with ΦC31 Integrase Transgenesis Techniques and Their Use to Generate New Notch Reporter Fly Lines. G3 (Bethesda)* **2,** *79–82 (2012).*

34. *Ward, E. J. et al. Stem cells signal to the niche through the Notch pathway in the Drosophila ovary. Curr Biol* **16,** *2352–2358 (2006).*

35. *Song, X., Call, G. B., Kirilly, D. & Xie, T. Notch signaling controls germline stem cell niche formation in the Drosophila ovary. Development* **134,** *1071–1080 (2007).*

36. *Grammont, M. & Irvine, K. D. fringe and Notch specify polar cell fate during Drosophila oogenesis. Development* **128,** *2243–2253 (2001).*

37. *Tworoger, M., Larkin, M. K., Bryant, Z. & Ruohola-Baker, H. Mosaic analysis in the drosophila ovary reveals a common hedgehog- inducible precursor stage for stalk and polar cells.* **151,** *739–48 (1999).*

38. *Besse, F. & Pret, A. M. Apoptosis-mediated cell death within the ovarian polar cell lineage of Drosophila melanogaster. Development* **130,** *1017–1027 (2003).*

39. *Borensztejn, A., Boissoneau, E., Fernandez, G., Agnès, F. & Pret, A. M. JAK/STAT autocontrol of ligand-producing cell number through apoptosis. Development* **140,** *195–204 (2013).*

40. *Liu, Z. et al. Coordinated niche-associated signals promote germline homeostasis in the Drosophila ovary. J Cell Biol* **211,** *469–484 (2015).*

41. *Li, C. et al. Ci antagonizes Hippo signaling in the somatic cells of the ovary to drive germline stem cell differentiation. Cell Res* **25,** *1152–1170 (2015).*

42. *Sun, J. & Deng, W. M. Hindsight mediates the role of notch in suppressing hedgehog signaling and cell proliferation. Dev Cell* **12,** *431–442 (2007).*

43. *López-Schier, H. & St Johnston, D. Delta signaling from the germ line controls the proliferation and differentiation of the somatic follicle cells during Drosophila oogenesis. Genes Dev* **15,** *1393–1405 (2001).*

21

534   44. *Grammont, M. & Irvine, K. D. Organizer activity of the polar cells during Drosophila oogenesis.*
535   *Development* **129,** *5131–5140 (2002).*
536   45. *Hsu, Y. C., Li, L. & Fuchs, E. Emerging interactions between skin stem cells and their niches. Nat*
537   *Med* **20,** *847–856 (2014).*
538   46. *Tan, D. W. & Barker, N. Intestinal stem cells and their defining niche. Curr Top Dev Biol* **107,** *77–*
539   *107 (2014).*
540   47. *Campbell, C., Risueno, R. M., Salati, S., Guezguez, B. & Bhatia, M. Signal control of hematopoietic*
541   *stem cell fate: Wnt, Notch, and Hedgehog as the usual suspects. Curr Opin Hematol* **15,** *319–325*
542   *(2008).*
543   48. *Takebe, N. et al. Targeting Notch, Hedgehog, and Wnt pathways in cancer stem cells: clinical*
544   *update. Nat Rev Clin Oncol* **12,** *445–464 (2015).*
545   49. *Haack, T., Bergstralh, D. T. & St Johnston, D. Damage to the Drosophila follicle cell epithelium*
546   *produces "false clones" with apparent polarity phenotypes. Biology open* **2,** *1313–1320 (2013).*
547   50. *Kambadur, R. et al. Regulation of POU genes by castor and hunchback establishes layered*
548   *compartments in the Drosophila CNS. Genes Dev* **12,** *246–260 (1998).*
549   51. *Schindelin, J. et al. Fiji: an open-source platform for biological-image analysis. Nat Methods* **9,**
550   *676–682 (2012).*
551
552

Acknowledgements

Author Contributions

W.D., A.P. and T.K. performed the experiments. W.D., A.P. and D.J. M. prepared the manuscript. All authors participated in the design of the experiments, the interpretation of the data, and the production of the final manuscript.

Competing Financial Interests statement

The authors declare no competing final interests.

570   **Figure Legends**

571   **Figure 1. *Axn* mutant clones cause supernumerary polar cells.**

572   (**a**) Drawing of a Drosophila ovariole in the sagittal view. Scale bar, 100 μm. (**b**) Sagittal view of stage

573   10 egg chambers with control (left panel) or FRT82B, *Axn^{1511}* mosaic (right panel) border cell clusters

574   (dashed boxes). Scale bar, 50 μm. (**c**) 3D projection view of border cell clusters containing FRT82B

575   control or FRT82B, *Axn^{1511}* mosaic clones. Homozygous mutant cells are RFP-negative (RFP$^-$). Polar

576   cells are identified by absence of Eya expression (dotted circles). Scale bar, 10 μm. (**d**) Quantification of

577   all border cell clusters in stage 9/10 egg chambers, regardless of whether they have clones or not, in

578   FRT82B control or FRT82B, *Axn^{1511}*, 4-5 days after clone induction. Data from n = 284 egg chambers

579   for control, 222 for *Axn$^-$*. Each dot represents one border cell cluster. Lines show the median with

580   interquartile range. (**e**) Border cell cluster in FRT42D control or FRT42D, *ptc^{S2}* mutant clones.

581   Homozygous mutant cells are RFP$^-$. Polar cells are Eya$^-$ (dotted circles). Scale bar, 10 μm.

582

583   **Figure 2. Differential effects of Wnt and Hh hyper-activation on follicle cell differentiation.**

584   (**a**) 3D projection view of one half of a wild type ovariole from the germarium to stage 4, stained with

585   Eya (green) and Cas (magenta) antibodies. Individual channels are shown in black and white. (**b**)

586   Quantification of Eya and Cas fluorescence intensity in all somatic cells in germarium regions 1-3 and in

587   stage 1-4 egg chambers. Data from n = 2,122 cells from 3 ovarioles per stage. Each dot represents one

588   cell. Data were normalized to maximum Eya or Cas intensity per ovariole. (**c**) Stage 4 egg chambers

589   with FRT82B control mosaic FSC clones compared to FRT82B, *Axn^{1511}* or FRT82B, *Apc2^{g10}, Apc^{Q8}*.

590   Homozygous mutant cells in the main body and anterior stalk regions are outlined (GFP$^+$, dashed lines).

591   Eya$^+$ GFP$^-$ cells appear in the outlined *Apc$^-$* clone due to Z stack projection. (**d**) Stage 4 egg chambers

592   with FRT42D control, FRT42D, *ptc^{S2}* or FRT42D, *cos^{H29}* mosaic FSC clones. Homozygous mutant cells

593   are RFP$^-$ (dashed lines). (**e-f**) Quantification of Eya and Cas fluorescence intensity in mosaic FSC

594   clones. Data from n = 1,222-1,447 cells from 4 stage 4 egg chambers per genotype. Data were

24

595   normalized to maximum Eya or Cas intensity in control cells per egg chamber. Scale bars, 20 μm. A.U.,

596   arbitrary unit.

597

598   **Figure 3. Independent actions of Wnt and Hh.**

599   (**a**) 3D projection view of one half of a germarium expressing the Wnt activity reporter *fz3-RFP* and

600   stained for Eya. RFP intensity is displayed using the "Physics" lookup table. (**b**) Quantification of Wnt

601   reporter intensity in all somatic cells from region 2-3 along the anterior-posterior axis. Data from n =

602   276 cells from 3 germaria. Each dot represents one cell. The three colours represent the three different

603   germaria. (**c**) Wnt reporter activity in germaria with *armRNAi*, $Axn^{S044230}$, smo^{D16}, or ptc^{S2} mutant clones

604   (red diamonds) compared to control cells in the same germarium (blue triangles). R^2 quantifies goodness

605   of fit of nonlinear regression. (**d**) Quantification of Wnt reporter activity in germaria with mosaic clones.

606   Data (median with interquartile range) from n = 16-103 cells from 3 germaria per genotype. Data were

607   normalized to the predicted value on the one phase decay curve fitted on the internal control cells. (**e**) A

608   germarium expressing the Hh activity reporter *ptc-GFP*. (**f**) Quantification of Hh reporter intensity in all

609   somatic cells from region 2 - 3 along the anterior-posterior axis. Data from n = 314 cells from 3

610   germaria. (**g**) Hh reporter activity in germaria with *smoRNAi*, *cosRNAi*, dsh^3, or $Axn^{S044230}$ mutant

611   clones. (**h**) Quantification of Hh reporter activity in germarium with mosaic clones. Data (median with

612   interquartile range) from n = 18-105 cells from 3 germaria per genotype. Scale bars, 10 μm. A.U.,

613   arbitrary unit. **, $p < 0.01$; ****, $p < 0.0001$; Samples labelled with different letters are significantly

614   different at $p < 0.01$.

615

616   **Figure 4. Wnt signalling in differentiating progenitor cells inhibits expression of the main body**

617   **cell fate determinant Eya.**

618   (**a**) 3D projection view of one half of ovarioles with FRT82B control or FRT82B, $Axn^{S044230}$ mutant

619   (GFP+, dashed lines) FSC clones stained with Eya and Cas. Arrowheads point to control polar cells in

25

620   stage 4 of *Axn⁻*, and arrows points to the mutant polar cells. Eya⁺ GFP⁻ cells appear in the outlined stage

621   4 clones due to Z stack projection. (**b**) Quantification of the percentage of stage 3-5 egg chambers with

622   Cas⁺ only clones. Data (mean $\pm$ SD) from n = 3 experiments, 77-89 egg chambers per genotype. *p* <

623   0.0001. (**c**) Quantification of percentage of main body or polar/stalk regions with cells expressing

624   cleaved death caspase-1 (cDcp1⁺) in FRT82B control or FRT82B, *Axn^{S044230}* mutant FSC clones. Data

625   (mean $\pm$ SD) from n = 3 experiments, 24-36 region 3-stage 2 egg chambers per group. *p* < 0.05. (**d**)

626   Sagittal confocal section of a stage 3 egg chamber with stalk region containing control cells (GFP⁻,

627   arrowhead) compared to *Axn^{S044230}* homozygous mutant, ectopic Cas⁺ cells (GFP⁺, dashed lines). (**e**) 3D

628   projection view of one half of a stage 1 egg chamber with *Axn^{S044230}* FSC clones (GFP⁺, dashed lines)

629   stained for Eya and Cas. (**f**) Quantification of Eya and Cas intensity in internal control or *Axn^{S044230}*

630   homozygous mutant main body cells in region 3/stage1. Data (median with interquartile range) from n =

631   3 egg chambers, 59 cells for control, 17 cells for *Axn⁻*. Data were normalized to average Eya or Cas in

632   internal control cells. ****, *p* < 0.0001. (**g**) Quantification of Eya and Cas intensity in germarium region

633   2b containing FRT82B control, *Axn^{S044230}*, *Axn^{S044230}* + *armRNAi*, *dsh³*, or *eyaRNAi* FSC clones. Data

634   (median with interquartile range) from n = 25-100 cells from 3-4 germaria per genotype. *p* < 0.0001. (**h**)

635   Quantification of Eya and Cas intensity in follicle cells with *Axn^{S044230}*, *eyaRNAi*, *UAS-eya*, or *Axn^{S044230}*

636   + *UAS-eya* mosaic FSC clones. Data from n = 1,365-1,434 cells from 4 stage 4 egg chambers per

637   genotype. Scale bar, 10 μm. A.U., arbitrary unit. Samples labelled with different letters are significantly

638   different.

639

640   **Figure 5. Notch activity in the germarium promotes polar cell specification.**

641   (**a**) NRE-GFP pattern from the germarium to stage 4 egg chambers. Arrows point to Notch activity in

642   the cap cells and region 2a/2b boundary cells and arrow-heads point to polar cells. (**b**) Quantification of

643   NRE-GFP intensity in cap cells, escort cells, and follicle cells along the anterior-posterior axis until

644   stage 4. Data from n= 1533 cells in 3 ovarioles. Different colours represent different ovarioles. Data

26

645   were normalized to maximum NRE-GFP intensity per sample. (**c**) NRE-GFP in $Axn^{S044230}$ heterozygous

646   control or mutant polar cell clusters in stage 2 (left panel) or stage 6 (right panel) egg chambers. Mutant

647   cells are RFP⁻ (dashed lines). Arrowheads point to control polar cells, and arrows points to the mutant

648   polar cells. (**d**) Quantification of Eya and Cas intensity in germarium containing *notchRNAi* mosaic FSC

649   clones. Data from n = 21-45 cells from 3-4 germaria per region. Data were normalized to average Eya or

650   Cas intensity in internal control cells. ***, $p < 0.001$; ****, $p < 0.0001$. Scale bars, 20 μm. A.U.,

651   arbitrary unit.

652

653   **Figure 6. Hh signalling controls the timing of proliferation versus differentiation.**

654   (**a**) 3D projection view of ovarioles with ptc^{S2} heterozygous control or large homozygous mutant (RFP⁻)

655   FSC clones. Dashed lines mark the stalk region. Arrows point to connected polar and stalk regions, and

656   arrowheads point to separated regions. (**b**) Quantification of the number of anterior stalk cells from stage

657   2-5 egg chambers in ptc^{S2} heterozygous control or large homozygous mutant FSC clones. Data (median

658   with interquartile range) from n = 8-15 egg chambers. $p < 0.0001$. (**c-d**) Sagittal view of posterior

659   polar/stalk region in ptc^{S2} heterozygous control or homozygous mutant egg chambers. Dashed lines

660   mark the stalk region. Arrowheads point to control polar/stalk region, and arrows point to the mutant

661   region. (**e**) STAT activity shown by 10XStat-GFP in ptc^{S2} heterozygous control (arrowheads) or

662   homozygous mutant (arrows) stalk cell regions. (**f**) Quantification of cells with cleaved death caspase-1

663   (cDcp1⁺) in ptc^{S2} heterozygous control or homozygous mutant polar cell regions. Data (mean ± SD)

664   from n = 2 experiments, 84-156 stage 2-5 polar cell regions per genotype. (**g**) Quantification of Eya and

665   Cas intensity in germarium region 2b containing FRT40A control, smo^{D16}, smo^3, ptc^{S2}, or cos^{H29} mutant

666   FSC clones. Data (median with interquartile range) from n = 21-68 cells from 4-6 germaria per

667   genotype. Data were normalized to average Eya or Cas in internal control cells. $p < 0.0001$. A.U.,

668   arbitrary unit. (**h**) NRE-RFP in smo^3 mutant FSC clone in a germarium. Mutant cells are RFP⁻ (dashed

669   lines), and the precocious Eya⁻, NRE⁺, presumptive polar cell is marked by *. (**i**) Quantification of

27

670   mutant clone size in germarium with FRT40A control, smo^{D16}, smo^3, ptc^{S2}, or cos^{H29} mutant FSC clones.

671   Data (median with interquartile range) from n = 9-13 germaria, $p < 0.05$. Scale bars, 20 μm. Samples

672   labelled with different letters are significantly different.

673

674   **Figure 7. Wnt and Hh exert independent effects in egg chamber patterning.**

675   (**a**) *C306-Gal4* driven knockdown of *dsh* and/or *smo* in follicle precursor cells. Data (mean $\pm$ SD) from n

676   = 3 experiments, 145-189 ovarioles per genotype. (**b**) Quantification of stalk cells anterior to stage 4-5

677   egg chambers in FRT82B control, $Axn^{S044230}$, *cosRNAi,* or $Axn^{S044230}$ + *cosRNAi* mosaic FSC clones.

678   Data (median with interquartile range) from n = 7-9 egg chambers per genotype. (**c**) Quantification of

679   Eya and Cas intensity in follicle cells with $Axn^{S044230}$, *cosRNAi*, or $Axn^{S044230}$ + *cosRNAi* mosaic FSC

680   clones. Data from n = 890-1,017 cells from 3 stage 4 egg chambers per genotype. A.U., arbitrary unit.

681   (**d**) Model for Wnt, Hh, and Notch in follicle precursor cell differentiation in the germarium. Samples

682   labelled with different letters are significantly different at $p < 0.01$.

28
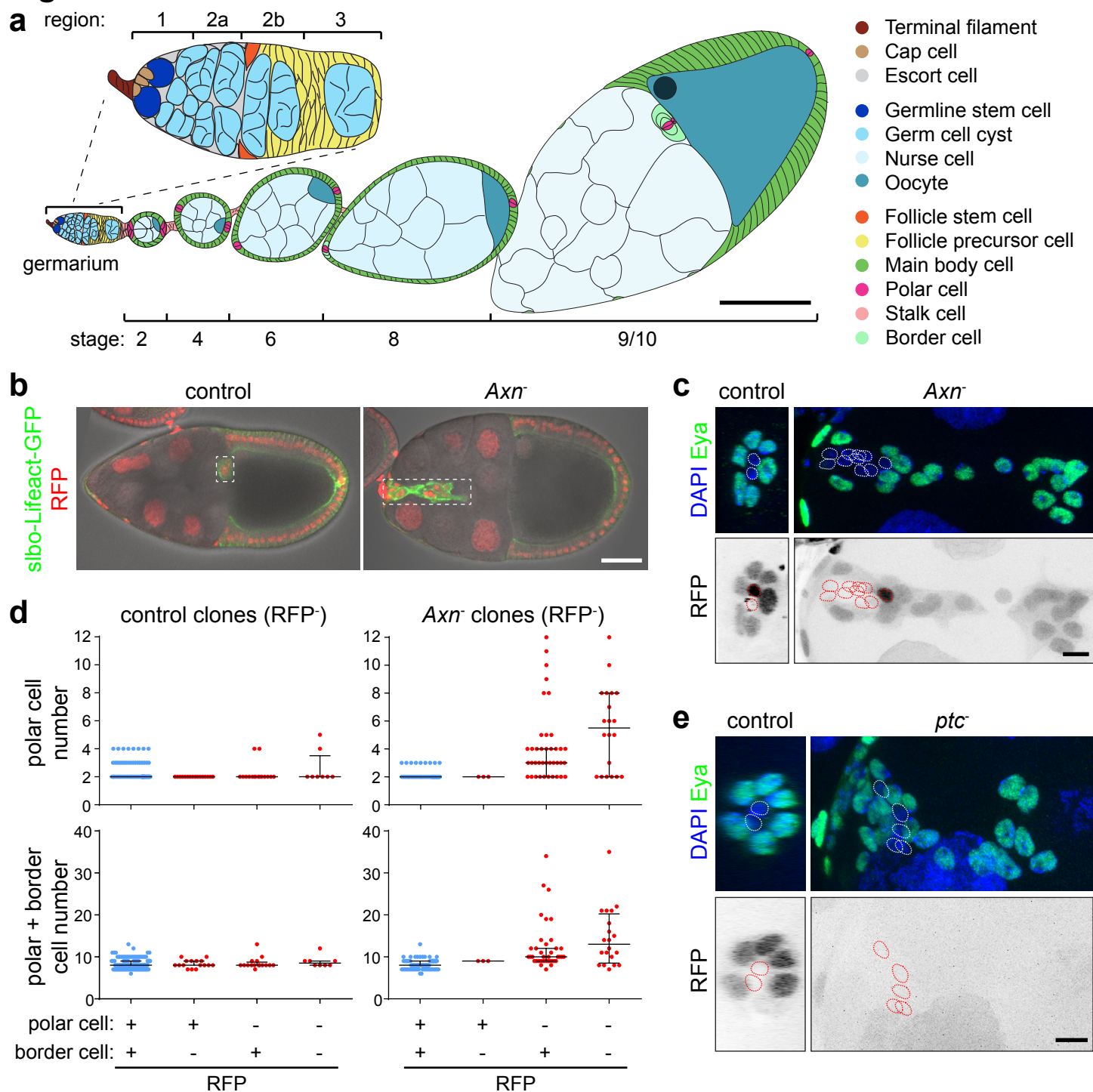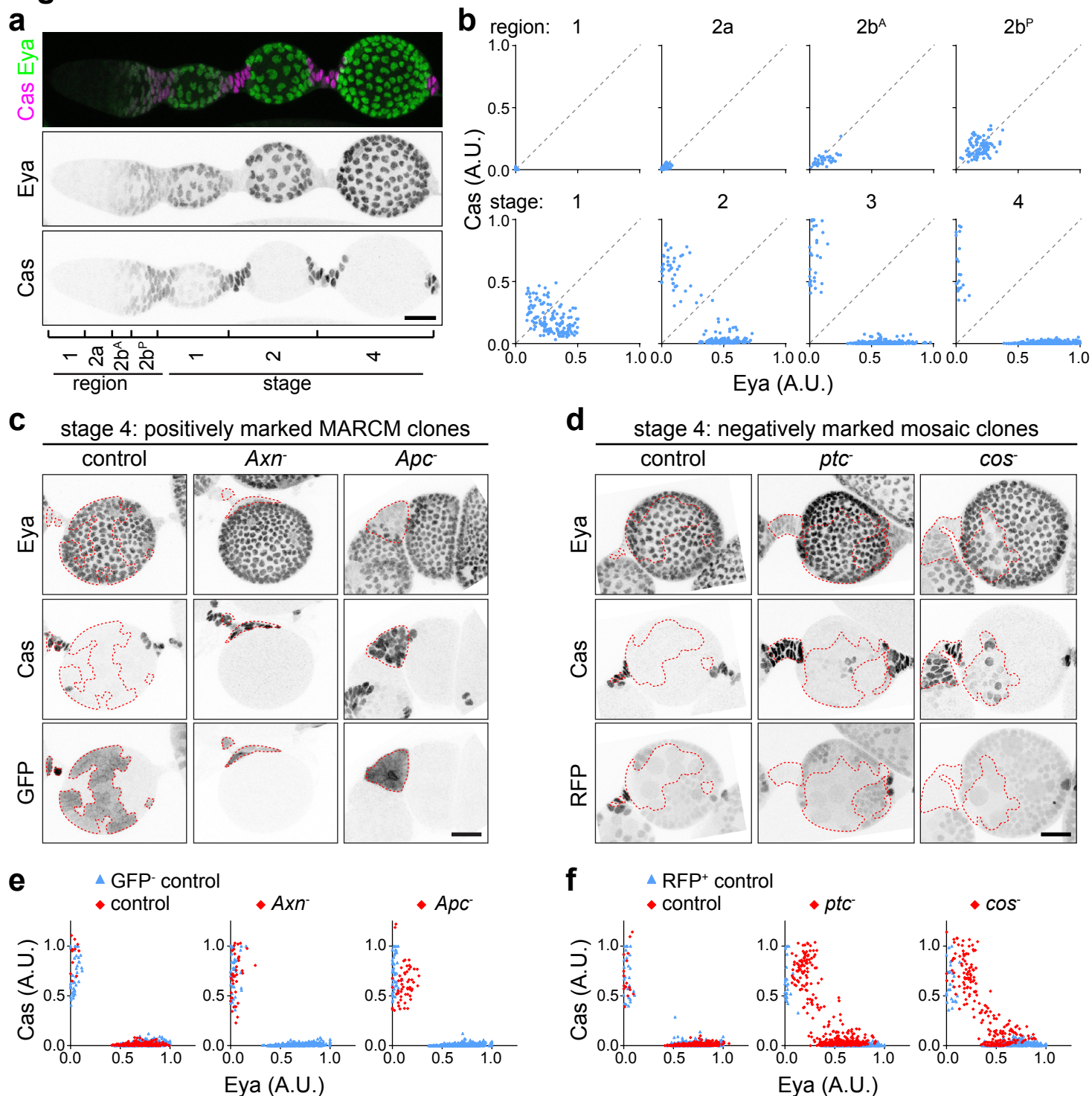
Figure 1

Figure 2

Figure 3
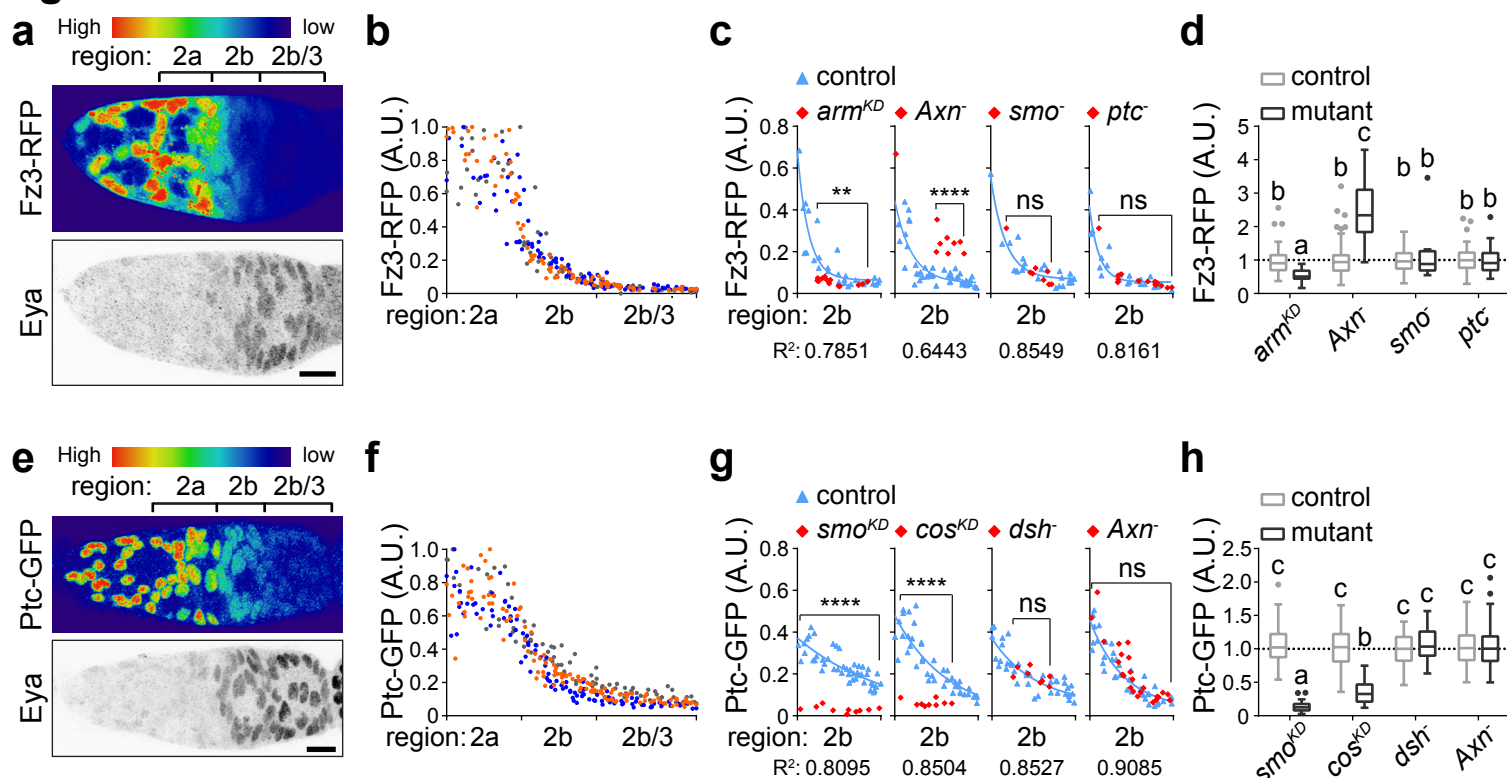
Figure 4
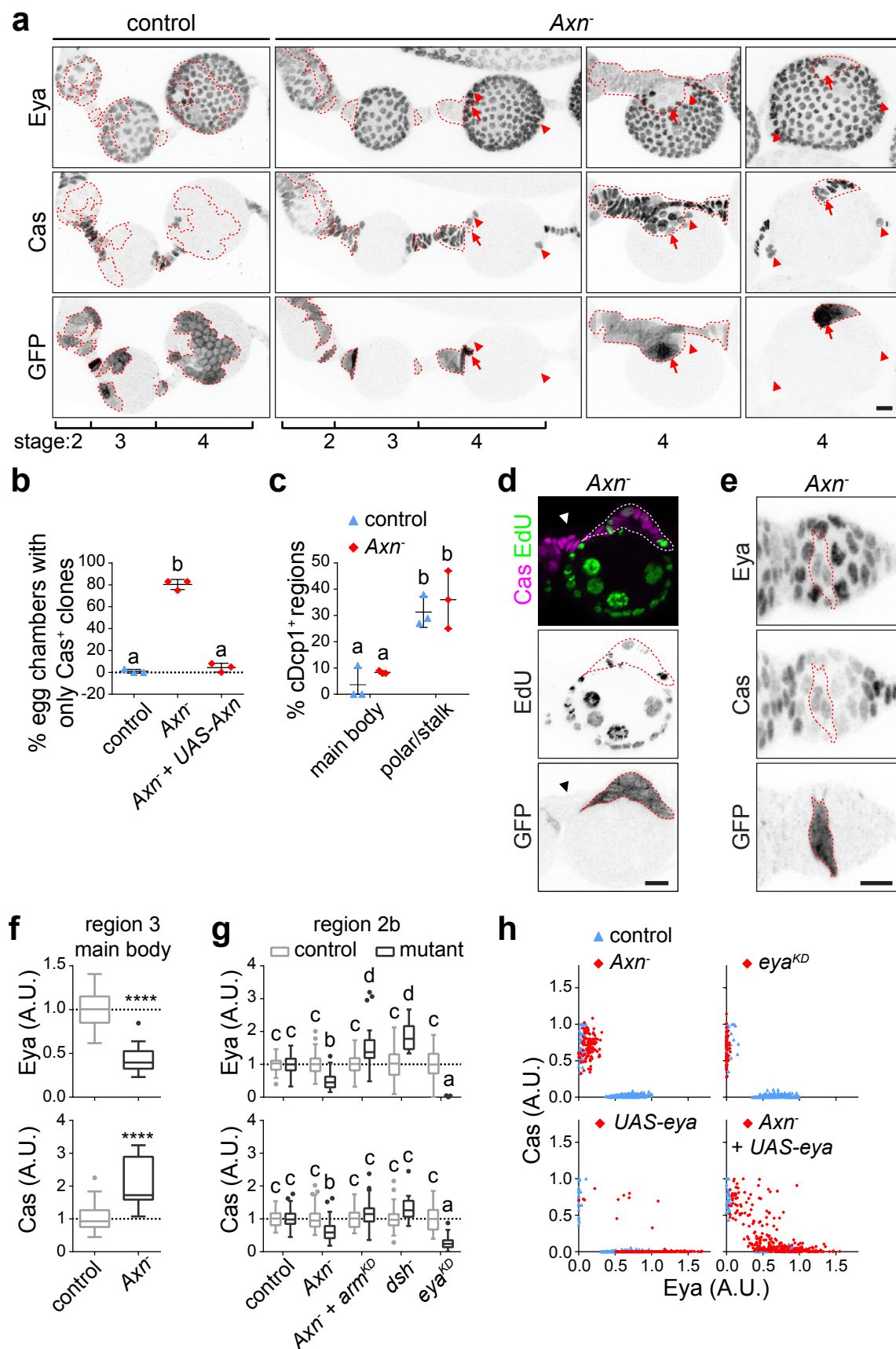
Figure 5

Figure 6

Figure 7

d

1. Wnt activity inhibits Eya expression
2. Hh activity promotes precursor proliferation
3. Hh activity inhibts precursor differentiation
4. Notch activity promotes precursor cross-migration
5. Notch activity promotes polar cell specification
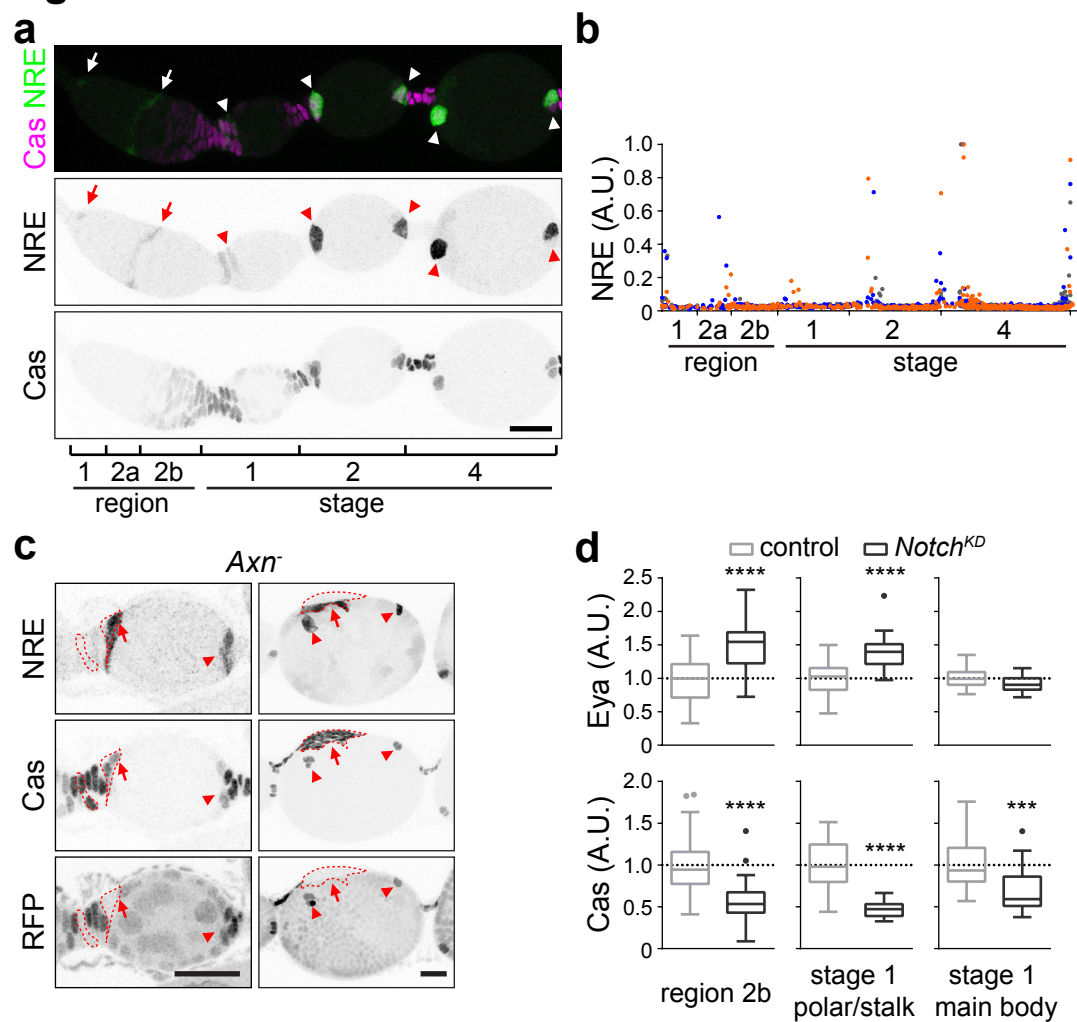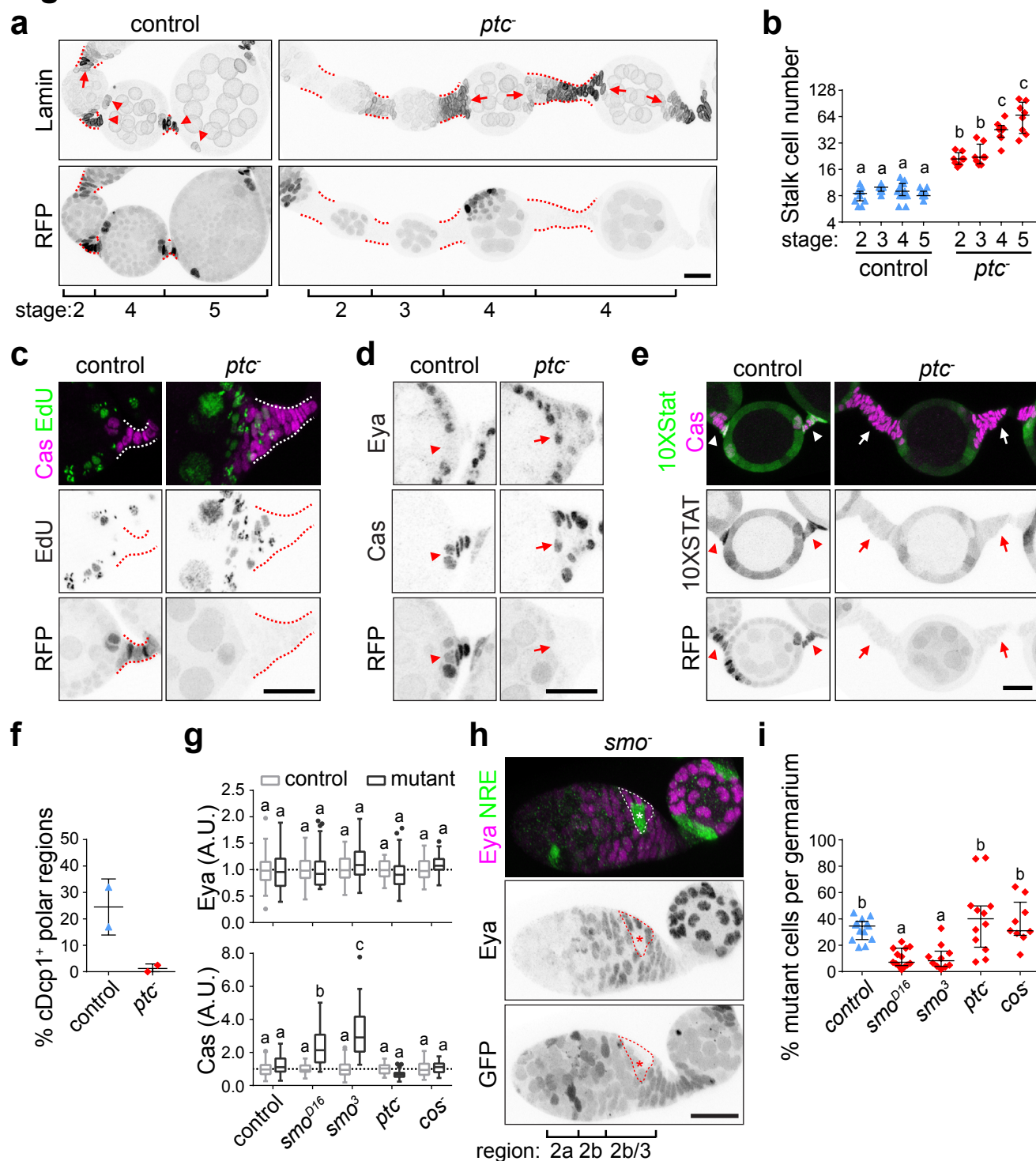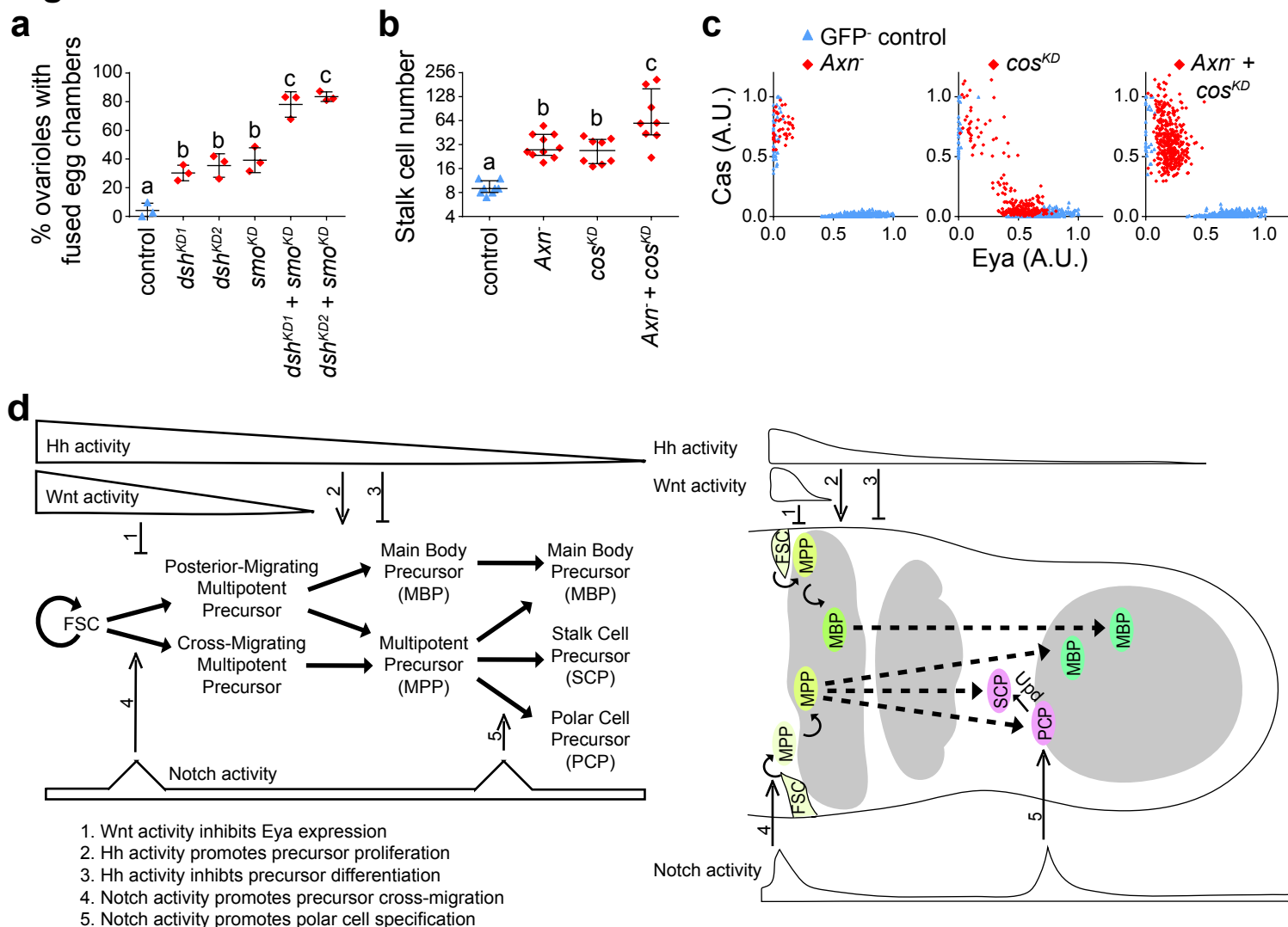
Supplementary Figure 1
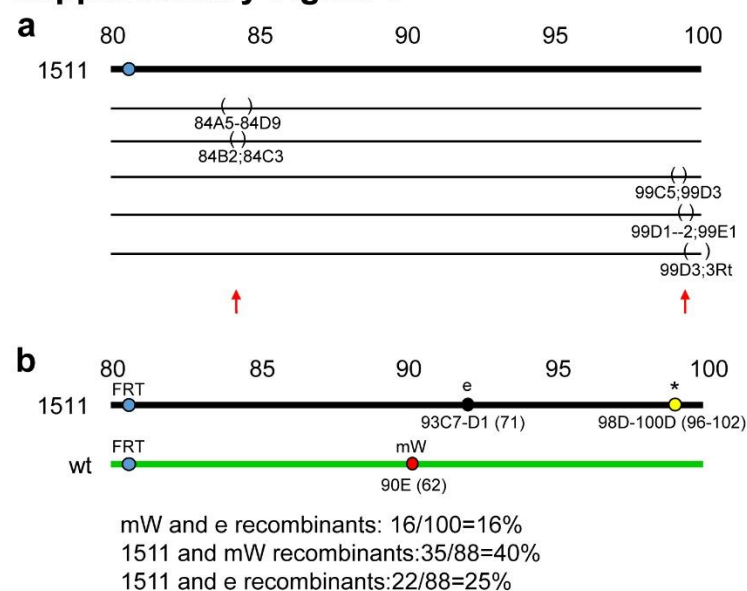
Supplementary Figure 1. Genetic mapping of Axn^{1511}.

(**a**) Mapping of Axn^{1511} by crossing to the chromosome 3R deficiency kit. Lethality was found when crossing 1511 to the 5 deficiency lines with the indicated deletions (brackets), which suggests that 1511 contains two lethal mutations (arrows). (**b**) Recombination mapping of Axn^{1511} by crossing to FRT82B, mW90E. The large border cell cluster phenotype (1511), red eye color (mW), and dark body color (e) were scored in recombinant lines. 1511 was mapped to chromosomal position 96-102 as estimated by recombination rates. The lethal mutation at chromosomal position 84 was removed in the recombinant used in Figure 1 and 2.

Supplementary Figure 2
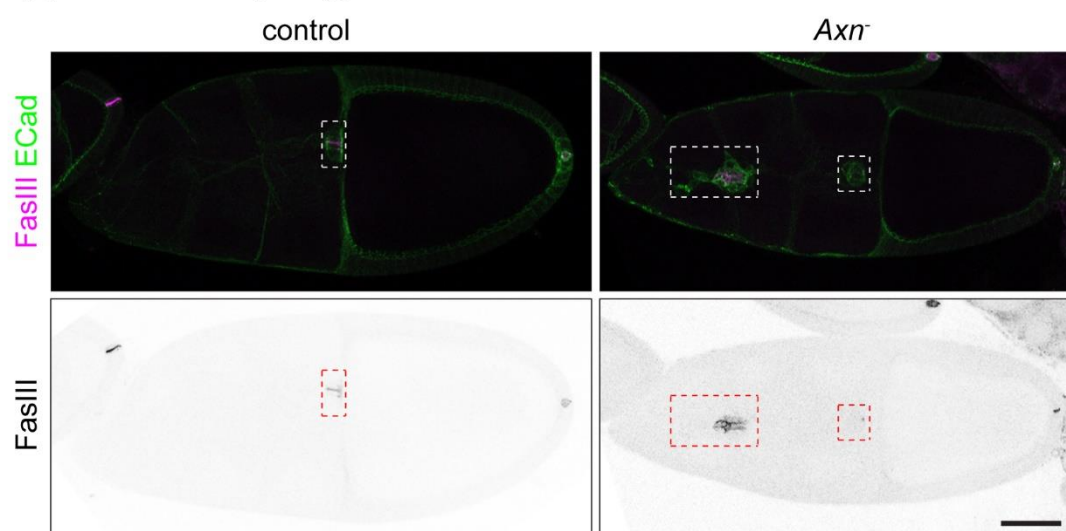
Supplementary Figure 2. $Axn^{S044230}$ mutant clones cause supernumerary polar cells.

Border cell clusters (dashed boxes) in FRT82B control or FRT82B, $Axn^{S044230}$ mosaic stage 10 egg chambers. ECad enriches in border cell clusters and FasIII accumulates on polar cell membrane. Scale bar, 50 μm.
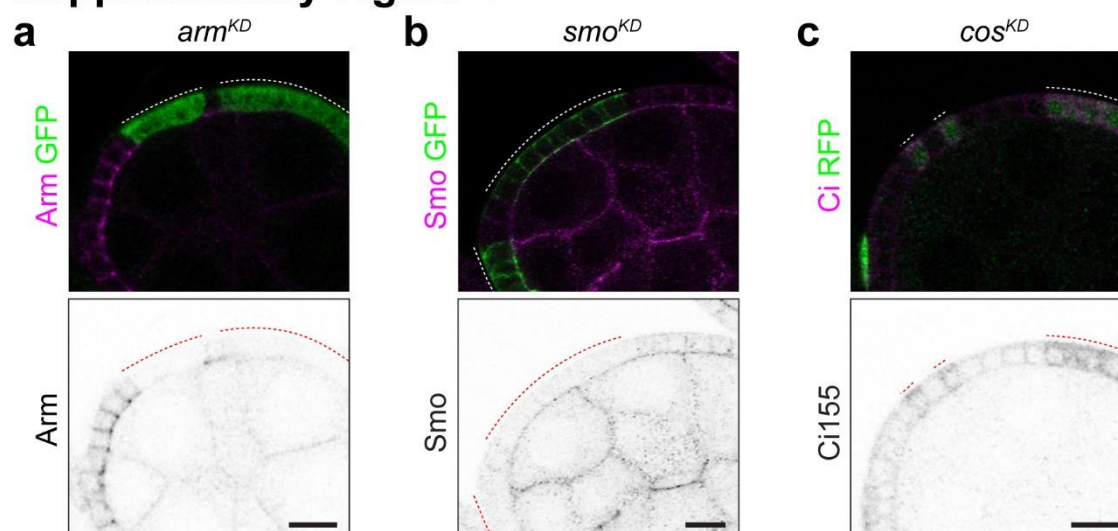
Supplementary Figure 3
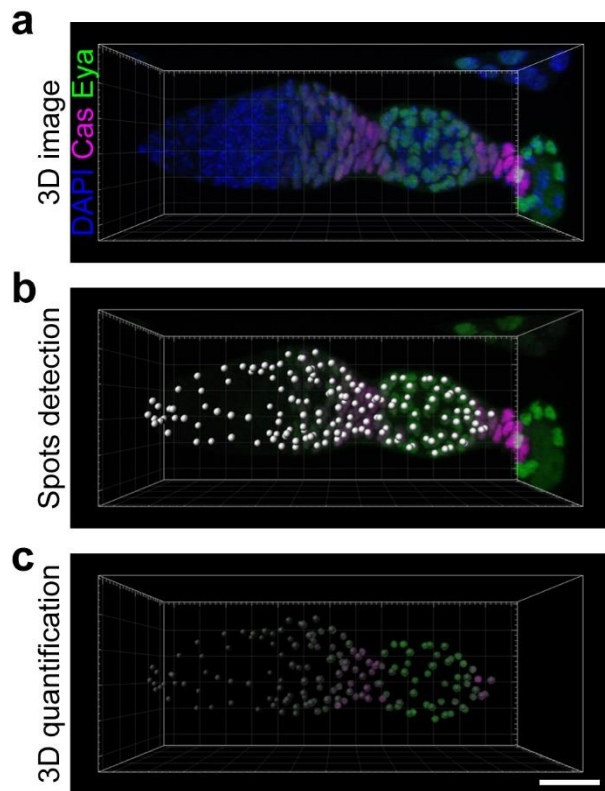
Supplementary Figure 3. Example of 3D quantification of the levels of both Eya and Cas in every somatic cell in a germarium.

(**a**) Image in 3D view. (**b**) Nuclei of somatic cells were first automatically detected by 2.5 μm spots (white dots) using the Eya channel, followed by manual proof editing using the Eya and DAPI channels to ensure one spot per nucleus. (**c**) A masked channel was created by setting the outside of the 2.5 μm spots to 0 intensity, and a 1.75 μm spot (semi-transparent dots) was automatically placed in the center of the 2.5 μm spot to get a strong and even nuclei intensity measurement. See methods for further details. Scale bar, 20 μm.
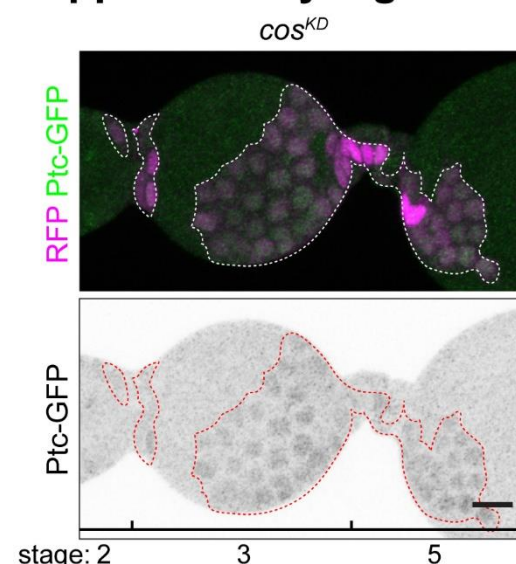
Supplementary Figure 4

Supplementary Figure 4. Validation of RNAi lines used.

(**a**) Sagittal confocal section of *armRNAi* flip-out clones (GFP⁺, indicated by the dashed line) in a stage 5 egg chamber stained with anti-Arm antibody (magenta in top panel, black in bottom). (**b**) Sagittal confocal section of *smoRNAi* flip-out clones (GFP⁺) in a stage 6 egg chamber stained with anti-Smo antibody (magenta in top panel, black in bottom). (**c**) Sagittal confocal section of *cosRNAi* flip-out clones (RFP⁺) in a stage 5 egg chamber stained with anti-Ci155 antibody (magenta in top panel, black in bottom). Scale bars, 10 μm.
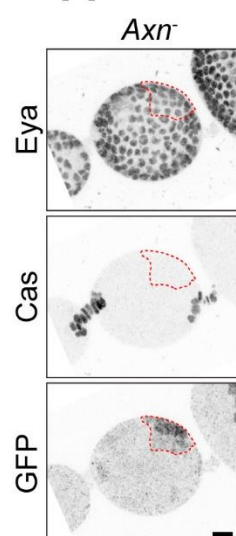
Supplementary Figure 5

Supplementary Figure 5. *ptc-GFP* signal in *cos^KD* ovariole.

3D projection view of one half of stage 3-5 egg chambers with *cosRNAi* flip-out clones (RFP⁺) showing the effect on expression of the *ptc-GFP* reporter. Scale bar, 10 μm.
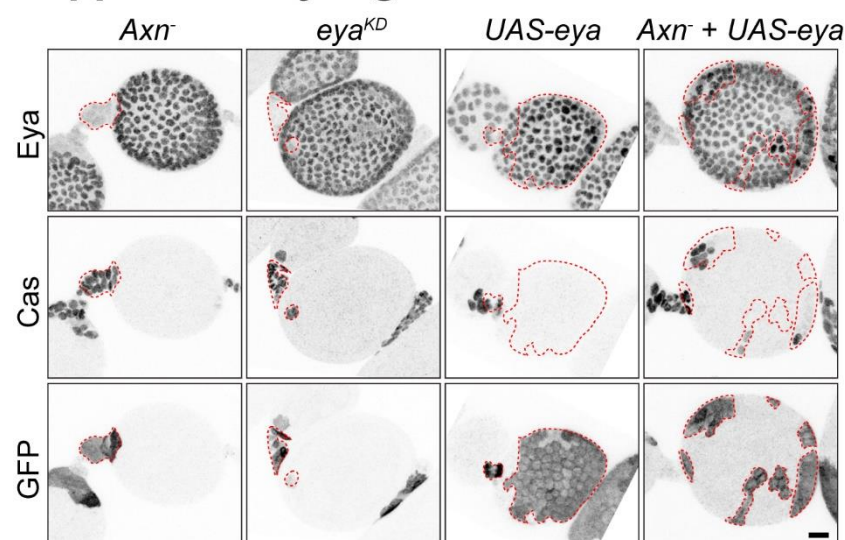
3

Supplementary Figure 6

Supplementary Figure 6. *Axn^{S044230}* transient clone does not bias towards polar/stalk fate.

3D projection view of one half of egg chambers with *Axn^{S044230}* transient clones 2 days post clone induction (GFP$^+$, dashed lines) stained for Eya and Cas. Scale bar, 10 μm.
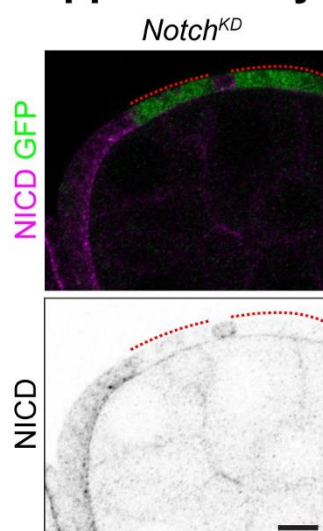
Supplementary Figure 7

Supplementary Figure 7. Reduction of Eya is the key cause for the cell fate change in *Axn^-*.

3D projection view of one half of stage 4 egg chambers with *Axn^{S044230}, eyaRNAi, UAS-eya*, or *Axn^{S044230}* + *UAS-eya* mosaic FSC clones (GFP$^+$). Scale bar, 10 μm.
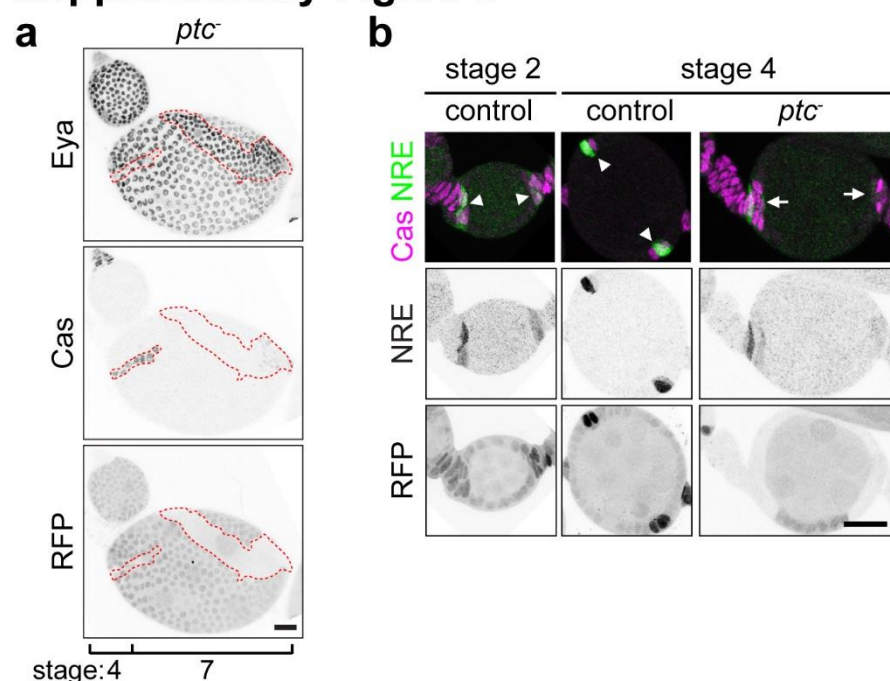
4

Supplementary Figure 8

47

48 **Supplementary Figure 8. Validation of *notchRNAi*.**

49 Sagittal confocal section of *notchRNAi* flip-out clones (GFP⁺) in a stage 6 egg chamber. Scale bar, 10
50 μm.

Supplementary Figure 9

Supplementary Figure 9. Hh hyper-activation delays follicle cell differentiation.

(**a**) 3D projection view of the follicle cell layer in *ptc*^{S2} clones (RFP$^-$). in a stage 7 egg chamber. (**b**) Notch activity shown by NRE-GFP in *ptc*^{S2} heterozygous control (arrowheads) or homozygous mutant (arrows) polar cell regions. Scale bars, 20 μm.
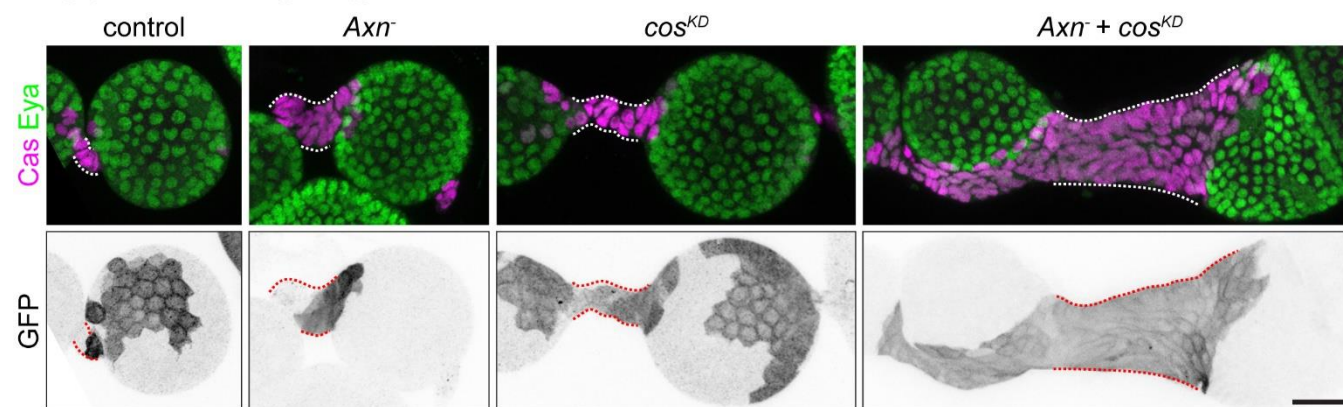
Supplementary Figure 10
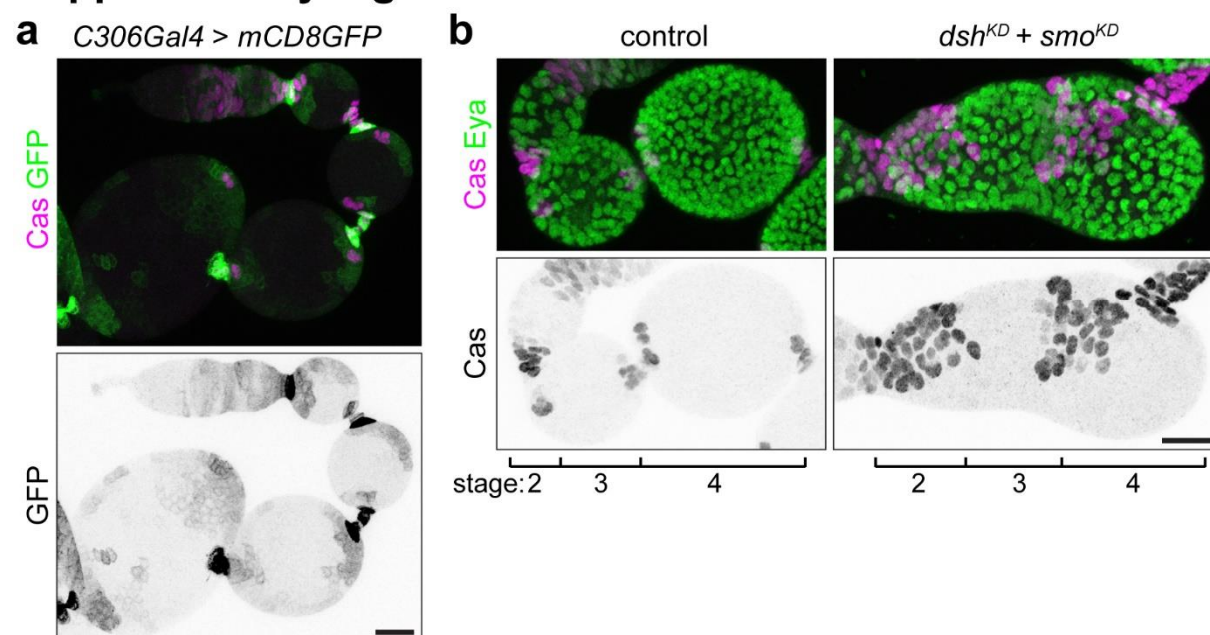
Supplementary Figure 10. C306 driven knockdown in follicle precursor cells.

(**a**) 3D projection view of an ovariole expressing *C306-Gal4* > mCD8GFP. (**b**) 3D projection view of ovarioles with stage 2, 3, 4 egg chambers in *C306-Gal4* > mCD8GFP control or *C306-Gal4* > dshRNAi + smoRNAi. Scale bars, 20 μm.

Supplementary Figure 11

Supplementary Figure 11. Supernumerary stalk caused by *Axn* and *cos* mutant.

3D projection view of one half of stage 4 egg chambers with FRT82B control, *Axn^{S044230}*, *cosRNAi,* or *Axn^{S044230}* + *cosRNAi* mosaic FSC clones. Scale bar, 20 μm.

Supplementary Table 1: List of fly stains used in this study

Purpose	Genotype	Source	Reference
mutant	w;FRT82B,w+,Axn[1511]/TM3	outcross original mutant line FRT82B,*75G4,e/TM3,e to w; FRT82b,w+ and move the lethality allele at 84B2;84C3	[1]
	w;FRT82B,Axn[S044230]/TM3	Mark Peifer, remove 2nd chromosome balancers	
	w; FRT82B, Apc2[g10], Apc[Q8]/TM3	Mark Peifer, remove 2nd chromosome balancers	[2]
	w,dsh[3],FRT19A/FM7a	BDSC6331	
	w;smo[D16],FRT40A/CyO	Andreas Bergmann, remove FLP	
	yw;smo[3],y+,dp,FRT40A/CyO	lab stock, remove eya allele	
	w;FRT42D,ptc[S2]/CyO	BDSC6332	
	yw;FRT42D,cos2[H29],y+w-/CyO	Andreas Bergmann	[3]
mosaic driver	ubi-RFPnls,w,FRT19A	BDSC31416	
	hsFLP,yw;ubi-GFPnls,FRT40A	combine BDSC1929 and BDSC5629	
	hsFLP,yw;FRT42D,ubi-RFPnls	combine BDSC1929 and BDSC35496	
	hsFLP,yw;FRT82B,ubi-RFPnls	lab stock	
	hsFLP,UAS-srcEGFP;actinGAL4,UAS-EGFP/CyO;FRT82B,armLacZ,tubGAL80/(MKRS)	Anna Jang	[4]
	hsFLP,yw;AyGal4,UAS-GFP (II)	combine BDSC1929 and BDSC4411	
	hsFLP;ActGal4(FRT.CD2),UAS-RFP/TM3	combine BDSC26902 and BDSC30558	
	hsFLP;AyGal4,UAS-moeGFP (III)	lab stock	
	yw;y+,FRT40A	BDSC1816	
	FRT42D;ry[605]	BDSC1802	
	w;FRT42D,w+	BDSC1928	
	w;FRT82B,w+	BDSC2050	
Gal4	C306Gal4;tubGal80ts	lab stock	
signaling reporter	w;fz3RFP (II)	Andrea Page-McCaw	[5]
	w;fz3RFP (III)	Erika Bach	[5]
	w;ptc-pelican/CyO	Todd Nystul	[6]
	w;NRE-pGR (III)	Sarah Bray	[7]
	w;NRE-pRR (III)	Sarah Bray	[7]
	w;10XStat-GFP (III)	BDSC26198	
fluorescent reporter	w;UAS-slbolifeactGFP (II)	lab stock	
	yw;UAS-mCD8GFP (II)	lab stock	
	w;UAS-GFPnls (III)	BDSC4776	
	w;UAS-AxnV5	Yashi Ahmed	

UAS transgene	w;UAS-eya/(CyO)	Ilaria Rebay	[8]
RNAi	y,sr,v;eyaRNAi(57314) (II)	BDSC57314	
	yw;armRNAi(107344) (II)	VDRC107344	
	y,v;dshRNAi(31306) (III)	BDSC31306	
	y,v;dshRNAi(31307) (III)	BDSC31307	
	yw;cosRNAi(108914) (II)	VDRC108914	
	y,v;smoRNAi(62987) (II)	BDSC62987	
	w;NotchRNAi(1112)	VDRC1112	

67

Supplementary Table 2: List of fly genotypes used in each experiment

Figure	Panel	Group	Genotype
1	A		hsFLP,yw/+;FRT42D,ubi-RFPnls/FRT42D,ry
	B	control	hsFLP,yw/w;slbolifeactGFP/+;FRT82B,ubi-RFPnls/+
		Axn^-	hsFLP,yw/w;slbolifeactGFP/+;FRT82B,ubi-RFPnls/FRT82B,w+,Axn[1511]
	C D	control	hsFLP,yw/w;FRT82B,ubi-RFPnls/FRT82B,w+
		Axn^-	hsFLP,yw/w;FRT82B,ubi-RFPnls/FRT82B,w+,Axn[1511]
	E	control	hsFLP,yw/+;FRT42D,ubi-RFPnls/FRT42D,w+
		ptc^-	hsFLP,yw/w;FRT42D,ubi-RFPnls/FRT42D,ptc[S2]
S1	A		FRT82B,*75G4,e/TM3,e crossed to 108 BDSC 3R deficiency lines
	B		w;FRT82B,w+/FRT82B,*75G4,e crossed to w; TM3/TM6B
S2		control	hsFLP,yw/w;FRT82B,ubi-RFPnls/FRT82B,w+
		Axn^-	hsFLP,yw/w;FRT82B,ubi-RFPnls/FRT82B,Axn[S044230]
2	A B		w;NRE-pGR (III)/+
	C E	control	hsFLP,UAS-srcEGFP/w;actinGAL4,UAS-EGFP/+;FRT82B,armLacZ,tubGAL80/FRT82B,w+
		Axn^-	hsFLP,UAS-srcEGFP/w;actinGAL4,UAS-EGFP/+;FRT82B,armLacZ,tubGAL80/FRT82B,w+,Axn[1511]
		Apc^-	hsFLP,UAS-srcEGFP/w;actinGAL4, UAS-EGFP/+;FRT82B,armLacZ,tubGAL80/FRT82B,Apc2[g10],Apc[Q8]
	D F	control	hsFLP,yw/+;FRT42D,ubi-RFPnls/FRT42D;ry[605]/+
		ptc^-	hsFLP,yw/w;FRT42D,ubi-RFPnls/FRT42D,ptc[S2]
		cos^-	hsFLP,yw/+;FRT42D,ubi-RFPnls/FRT42D,cos2[H29]
S3			w;NRE-pGR (III)/+
3	A B		w;fz3-RFP(II)/+
	C D	arm^{KD}	hsFLP/yw;AyGal4,UAS-GFP/armRNAi(107344);fz3-RFP/+
		Axn^-	hsFLP,UAS-srcEGFP/w;actinGAL4,UAS-EGFP/fz3-RFP;FRT82B,armLacZ,tubGAL80/FRT82B,Axn[S044230]
		smo^-	hsFLP,yw/w;ubi-GFPnls,FRT40A/smo[D16],FRT40A;fz3-RFP/+
		ptc^-	hsFLP,yw/w;FRT42D,ubi-GFPnls/FRT42D,ptc[S2];fz3-RFP/+
	E F		w;ptc-pelican-GFP(II)/+
	G H	smo^{KD}	hsFLP,yw/yv;ptc-pelican-GFP/smoRNAi(62987);ActGal4(FRT.CD2),UAS-RFP/+
		cos^{KD}	hsFLP,yw/yw;ptc-pelican-GFP/cosRNAi(108914);ActGal4(FRT.CD2),UAS-RFP/+
		dsh^-	ubi-RFPnls,w,FRT19A/w,dsh[3],FRT19A;ptc-pelican-GFP/+
		Axn^-	hsFLP,yw/w;ptc-pelican-GFP/+;FRT82B,ubi-RFPnls/FRT82B, Axn[S044230]
S4	A	arm^{KD}	hsFLP,yw/yw;AyGal4,UAS-GFP/armRNAi(107344)
	B	smo^{KD}	hsFLP,yw/yv;smoRNAi(62987)/+;AyGal4,UAS-moeGFP/+

	C	*cos^KD*	hsFLP,yw/yw;ptc-pelican-GFP/cosRNAi(108914);ActGal4(FRT.CD2),UAS-RFP/+
S5		*cos^KD*	hsFLP,yw/yw;ptc-pelican-GFP/cosRNAi(108914);ActGal4(FRT.CD2),UAS-RFP/+
4	A-F	control	hsFLP,UAS-srcEGFP/w;actinGAL4,UAS-EGFP/+;FRT82B,armLacZ,tubGAL80/FRT82B,w+
		Axn^-	hsFLP,UAS-srcEGFP/w;actinGAL4,UAS-EGFP/+;FRT82B,armLacZ,tubGAL80/FRT82B,Axn[S044230]
		Axn^- + UAS-Axn	hsFLP,UAS-srcEGFP/w;actinGAL4,UAS-EGFP/UAS-AxnV5;FRT82B,armLacZ,tubGAL80/FRT82B,Axn[S044230]
	G	control	hsFLP,UAS-srcEGFP/w;actinGAL4,UAS-EGFP/+;FRT82B,armLacZ,tubGAL80/FRT82B,w+
		Axn^-	hsFLP,UAS-srcEGFP/w;actinGAL4,UAS-EGFP/+;FRT82B,armLacZ,tubGAL80/FRT82B,Axn[S044230]
		Axn^- + arm^KD	hsFLP,UAS-srcEGFP/w;actinGAL4,UAS-EGFP/armRNAi(107344);FRT82B,armLacZ,tubGAL80/FRT82B,Axn[S044230]
		dsh^-	ubi-RFPnls,w,FRT19A/w,dsh[3],FRT19A
		eya^KD	hsFLP,yw/ysrv;AyGal4,UAS-GFP/eyaRNAi(57314)
	H	*Axn^-*	hsFLP,UAS-srcEGFP/w;actinGAL4,UAS-EGFP/+;FRT82B,armLacZ,tubGAL80/FRT82B,Axn[S044230]
		eya^KD	hsFLP,yw/ysrv;AyGal4,UAS-GFP/eyaRNAi(57314)
		UAS-eya	hsFLP,yw/w;AyGal4,UAS-GFP/UAS-eya
		Axn^- + UAS-eya	hsFLP,UAS-srcEGFP/w;actinGAL4,UAS-EGFP/UAS-eya;FRT82B,armLacZ,tubGAL80/FRT82B,Axn[S044230]
S6		*Axn^-*	hsFLP,UAS-srcEGFP/w;actinGAL4,UAS-EGFP/+;FRT82B,armLacZ,tubGAL80/FRT82B,Axn[S044230]
S7		*Axn^-*	hsFLP,UAS-srcEGFP/w;actinGAL4,UAS-EGFP/+;FRT82B,armLacZ,tubGAL80/FRT82B,Axn[S044230]
		eya^KD	hsFLP,yw/ysrv;AyGal4,UAS-GFP/eyaRNAi(57314)
		UAS-eya	hsFLP,yw/w;AyGal4,UAS-GFP/UAS-eya
		Axn^- + UAS-eya	hsFLP,UAS-srcEGFP/w;actinGAL4,UAS-EGFP/UAS-eya;FRT82B,armLacZ,tubGAL80/FRT82B,Axn[S044230]
5	A-B		w;NRE-pGR (II)/+
	C	*Axn^-*	hsFLP,yw/w;NRE-pGR/+;FRT82B,ubi-RFPnls/FRT82B,Axn[S044230]
	D	*Notch^KD*	hsFLP,UAS-srcEGFP/w;actinGAL4,UAS-EGFP/NotchRNAi(1112);FRT82B,armLacZ,tubGAL80/FRT82B,w+
S8		*Notch^KD*	hsFLP,yw/w;AyGal4,UAS-GFP/NotchRNAi(1112)
6	A-D F		hsFLP,yw/w;FRT42D,ubi-RFPnls/FRT42D,ptc[S2]
	E		hsFLP,yw/w;FRT42D,ubi-RFPnls/FRT42D,ptc[S2];10XStat-GFP/+
	G I	control	hsFLP,yw/yw;y+,FRT40A/ubi-GFPnls,FRT40A
		smo^D16	hsFLP,yw/w;ubi-GFPnls,FRT40A/smo[D16],FRT40A

11

		smo³	hsFLP,yw/yw;ubi;GFPnls,FRT40A/smo[s],y+,dp,FRT40A
		ptc⁻	hsFLP,yw/w;FRT42D,ubi-RFPnls/FRT42D,ptc[S2]
		cos⁻	hsFLP,yw/+;FRT42D,ubi-RFPnls/FRT42D,cos2[H29]
	H	*smo⁻*	hsFLP,yw/w;ubi-GFPnls,FRT40A/smo[3],y+,dp,FRT40A;NRE-pRR/+
S9	A	*ptc⁻*	hsFLP,yw/w;FRT42D,ubi-RFPnls/FRT42D,ptc[S2]
	B		hsFLP,yw/w;FRT42D,ubi-RFPnls/FRT42D,ptc[S2]
7	A	control	C306Gal4/w;Gal80ts/+;UAS-GFPnls/+
		dsh^KD1	C306Gal4/w;Gal80ts/+;dshRNAi(31306)/+
		dsh^KD2	C306Gal4/w;Gal80ts/+;dshRNAi(31307)/+
		smo^KD	C306Gal4/w;Gal80ts/smoRNAi(62987)
		dsh^KD1 + smo^KD	C306Gal4/w;Gal80ts/smoRNAi(62987);dshRNAi(31306)/+
		dsh^KD2 + smo^KD	C306Gal4/w;Gal80ts/smoRNAi(62987);dshRNAi(31307)/+
	B-C	control	hsFLP,UAS-srcEGFP/w;actinGAL4,UAS-EGFP/+;FRT82B,armLacZ,tubGAL80/FRT82B,w+
		Axn⁻	hsFLP,UAS-srcEGFP/w;actinGAL4,UAS-EGFP/+;FRT82B,armLacZ,tubGAL80/FRT82B,Axn[S044230]
		cos^KD	hsFLP,UAS-srcEGFP/yw;actinGAL4,UAS-EGFP/cosRNAi(108914);FRT82B,armLacZ,tubGAL80/FRT82B,w+
		Axn⁻ + cos^KD	hsFLP,UAS-srcEGFP/w;actinGAL4,UAS-EGFP/cosRNAi(108914);FRT82B,armLacZ,tubGAL80/FRT82B,Axn[S044230]
S10	A		C306Gal4/yw;UAS-mCD8GFP/+
	B	control	C306Gal4/w;Gal80ts/+;UAS-GFPnls/+
		dsh^KD + smo^KD	C306Gal4/w;Gal80ts/smoRNAi(62987);dshRNAi(31307)/+
S11		control	hsFLP,UAS-srcEGFP/w;actinGAL4,UAS-EGFP/+;FRT82B,armLacZ,tubGAL80/FRT82B,w+
		Axn⁻	hsFLP,UAS-srcEGFP/w;actinGAL4,UAS-EGFP/+;FRT82B,armLacZ,tubGAL80/FRT82B,Axn[S044230]
		cos^KD	hsFLP,UAS-srcEGFP/yw;actinGAL4,UAS-EGFP/cosRNAi(108914);FRT82B,armLacZ,tubGAL80/FRT82B,w+
		Axn⁻ + cos^KD	hsFLP,UAS-srcEGFP/w;actinGAL4,UAS-EGFP/cosRNAi(108914);FRT82B,armLacZ,tubGAL80/FRT82B,Axn[S044230]

69

Supplementary Table 3: Stage of egg chamber development

Stage*	Nurse cell nucleus diameter (µm)	
	anterior	posterior
2	5-7	
3	7-9	
4	9-12.5	
5	12.5-15.8	
6	15.8-18	
7	18-21.8	23-30
8	21.8-25	28-32
9	25-35	32-43
10	35-45	42-50

* Stage according to [9]

84 Bibliography

85 1. Silver, D. L. & Montell, D. J. Paracrine signaling through the JAK/STAT pathway activates invasive behavior of ovarian epithelial cells in Drosophila. *Cell*
86 **107,** 831–841 (2001).

87 2. Akong, K., McCartney, B. M. & Peifer, M. Drosophila APC2 and APC1 have overlapping roles in the larval brain despite their distinct intracellular
88 localizations. *Dev Biol* **250,** 71–90 (2002).

89 3. Christiansen, A. E. *et al.* Non-cell autonomous control of apoptosis by ligand-independent Hedgehog signaling in Drosophila. *Cell Death Differ* **20,**
90 302–311 (2013).

91 4. Chang, Y. C., Jang, A. C., Lin, C. H. & Montell, D. J. Castor is required for Hedgehog-dependent cell-fate specification and follicle stem cell maintenance
92 in Drosophila oogenesis. *Proc Natl Acad Sci U S A* **110,** E1734–42 (2013).

93 5. Olson, E. R. *et al.* Yan, an ETS-domain transcription factor, negatively modulates the Wingless pathway in the Drosophila eye. *EMBO Rep* **12,** 1047–
94 1054 (2011).

95 6. Sahai-Hernandez, P. & Nystul, T. G. A dynamic population of stromal cells contributes to the follicle stem cell niche in the Drosophila ovary.
96 *Development* **140,** 4490–4498 (2013).

97 7. Housden, B. E., Millen, K. & Bray, S. J. Drosophila Reporter Vectors Compatible with ΦC31 Integrase Transgenesis Techniques and Their Use to
98 Generate New Notch Reporter Fly Lines. *G3 (Bethesda)* **2,** 79–82 (2012).

99 8. Hsiao, F. C., Williams, A., Davies, E. L. & Rebay, I. Eyes absent mediates cross-talk between retinal determination genes and the receptor tyrosine
100 kinase signaling pathway. *Dev Cell* **1,** 51–61 (2001).

101 9. Spradling, A. C. in *The development of Drosophila melanogaster* 1–70 (Cold Spring Harbor Laboratory Press, 1993).

102